Bachelor Thesis:

Detection of Few-Photon Pulses for a Rydberg Quantum Optics Experiment

by
Fabian Böttcher

19. August 2013

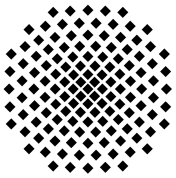

Universität Stuttgart

Prof. Dr. Tilman Pfau
Dr. Sebastian Hofferberth
5th Institute of Physics
University of Stuttgart

Decleration

I hereby declare that this thesis is my own work and that, to the best of my knowledge and belief, it contains no material previously published or written by another person, except where due acknowledgement has been made.

Filderstadt, 19. August 2013

Fabian Böttcher

Zusammenfassung

Lange Zeit war nicht geklärt was Licht tatsächlich ist. Bei der Untersuchung von Licht wurde die Frage aufgeworfen ob es sich bei Licht um ein Teilchen oder eine Welle handelt. Mit Maxwells Theorie des Elektromagnetismus, in welcher Licht als elektromagnetische Welle beschrieben werden konnte, schien die Frage beantwortet. Effekte wie der Fotoeffekt oder die Schwarzkörperstrahlung schienen dieser Auffassung jedoch zu widersprechen und wieder in Richtung von Lichtteilchen zu zeigen. Seit der Quantentheorie wissen wir jedoch, dass Licht sowohl als eine Welle als auch als ein Teilchen beschrieben werden kann. Die Quantisierung des Lichtfeldes führt zu den Elementarteilchen der elektromagnetischen Strahlung: den Photonen.
Mit modernen Messgeräten ist es möglich schwache Lichtsignale bis hin zu einzelnen Photonen zu messen. Im Verlauf dieser Arbeit werden einzelne Photonen mit zwei COUNT-250C-FC Einzelphotonenzähler der Firma Laser Components gemessen. Das Ziel dieser Arbeit bestand darin mit dem Umgang der Photonenzähler vertraut zu werden, diese auf ihre Verlässlichkeit zu prüfen und die benötigten Techniken und Programme für den späteren Einsatz im Experiment der Rydberg Quantum Optics (RQO) Gruppe zu entwickeln. Um dieses Ziel zu erreichen wurden die neu erworbenen Photonenzähler und der ebenfalls neue Time-Tagger zu Beginn der Arbeit getestet. Dazu wurde zuerst die Dunkelzählrate der Photonenzähler gemessen und daraufhin die statistische Verteilung von Photonen in einem Laserstrahl untersucht.
Als erste Anwendung wurden Lichtpulse mit einem mechanischen Shutter erzeugt und mit den Photonenzählern gemessen. Damit wurde der Shutter auf seine Zuverlässigkeit untersucht, was ergab dass dieser sehr verlässlich arbeitet. Daruafhin wurden Lichtpulse mit einem Akustooptischen Modulator erzeugt und vermessen.
Am Ende der Arbeit wurden die erlernten Techniken verwendet um die Verzögerung in einem Medium, welches elektromagnetisch induzierte Transparenz zeigt, zu messen. Diese Messung führte für die kalte Rubidium-Atomwolke des RQO Experiments zu Verzögerungszeiten von ca. 100 ns. Dieser Verzögerungszeit entsprechen Gruppengeschwindigkeiten von ca. $1000\,\frac{\mathrm{m}}{\mathrm{s}}$ des Lichtpulses in der Atomwolke.

Contents

1 Introduction

The nature of light has been a subject of interest for a long time in physics. In the centre of the investigation about the nature of light stood the question of whether light is described by a particle or a wave. With Maxwell's theory of electromagnetism and its description of light as an electromagnetic wave, this question seemed to be answered. However effects like the photoelectric effect or the black body radiation once again pointed in the direction of light as a particle. The answer to the question came with quantum theory and its wave-particle duality. Light can be described by both a particle and a wave.
The quantization of the light field leads to the elementary particle of radiation: the photon. Each photon carries an energy of $\hbar\omega$ from the electromagnetic field. With today's means of detection it's possible to detect weak light signals down to single photons.
During this thesis this is done using two COUNT-250C-FC single photon counting modules from Laser Components. With these counting modules light pulses are reconstructed from single photon counts through repeated measurements. The aim of this thesis was to work with the single photon counting modules and test their functionality, as they're necessary in the experiment of the Rydberg Quantum Optics group. To achieve this aim the new single photon counting modules together with the new Time-Tagger module were tested in the beginning of this thesis. With both modules the photon statistics of laser light, the reliability of a mechanical shutter and light pulses created with an acousto-optic modulator were investigated.
At the end of the thesis the learned methods were used to measure the delay, caused by a medium showing electromagnetically induced transparency for two different setups. In particular the delay of the Rubidium cloud in the setup of the Rydberg Quantum Optics group was measured.

2 Theory

In this chapter the relevant theory for the measurements done during this thesis is described. This chapter begins with an introduction to quantum optics, then addresses a short paragraph about pulses and in the end of the chapter a brief overview of electromagnetically induced transparency and slow light is presented.

2.1 Quantum Optics

In this section the theory of quantum optics is introduced. Starting from the classical description of light, the connection of light with an harmonic oscillator is used to introduce the quantization of the light field. In the end of this chapter the statistical properties of light as a stream of photons is investigated, leading to a classification of different light sources. This is done on the basis of the quantum optics books written by Mark Fox [1] and Rodney Loudon [2].

2.1.1 Classical Optics

Classically light is described as an electromagnetic wave. As such the description is based on the electric field $\vec{E}$ and magnetic field $\vec{B}$. In a medium there is also the electric displacement $\vec{D}$ and the magnetic $\vec{H}$-field, which are related to the electromagnetic fields as given by

$$\vec{D} = \epsilon_0 \left(1 + \chi_{\text{el}}\right) \vec{E} = \epsilon_0 \epsilon_r \, \vec{E} \tag{2.1}$$

and

$$\vec{B} = \mu_0 \left(1 + \chi_{\text{mag}}\right) \vec{H} = \mu_0 \mu_r \, \vec{H} \tag{2.2}$$

for a linear reacting medium. In these equation χ stands for the electric or the magnetic susceptibility, ϵ_0 for the permittivity of free space, ϵ_r for the relative permittivity of the medium, μ_0 for the permeability of free space and μ_r for the relative permeability of the medium. In most optical systems the relative permeability can be neglected ($\mu_r = 1$), because magnetic materials are too slow to respond at optical frequencies.

These quantities have to fulfil the Maxwell equations

$$\vec{\nabla} \cdot \vec{D} = \varrho \tag{2.3}$$

$$\vec{\nabla} \cdot \vec{B} = 0 \tag{2.4}$$

$$\vec{\nabla} \times \vec{E} = -\frac{\partial \vec{B}}{\partial t} \tag{2.5}$$

$$\vec{\nabla} \times \vec{H} = \vec{j} + \frac{\partial \vec{D}}{\partial t} \ , \tag{2.6}$$

with the charge density ϱ and the current density $\vec{j}$. In free space without charges and currents wave-like solutions of the Maxwell equations are possible. Taking the curl of equation 2.5, using the other Maxwell equations and vector identities, we get a wave equation for the electric field $\vec{E}$ (as seen in equation 2.7) and similar a wave equation for the magnetic field $\vec{B}$.

$$\nabla^2 \vec{E} = \mu_0 \mu_r \epsilon_0 \epsilon_r \frac{\partial^2 \vec{E}}{\partial t^2} \tag{2.7}$$

This equation describes an electromagnetic wave with its speed given by $1/v^2 = \mu_0 \mu_r \epsilon_0 \epsilon_r$. In free space the relative permittivity and the relative permeability are both equal to 1 and as such the speed is given by the vacuum light velocity $c = 1/\sqrt{\mu_0 \epsilon_0} = 299792458 \, \frac{\mathrm{m}}{\mathrm{s}}$. The easiest solutions of the wave equation are plane waves, with the angular frequency satisfying the dispersion relation $\omega = c\,k$, in which k is the absolute value of the wave vector.
In a medium the current density $\vec{j}$ does not have to vanish, even if the medium is not charged. Considering Ohm's law $\vec{j} = \sigma \vec{E}$, in which σ is the conductivity of the medium, a different wave equation can be derived.

$$\nabla^2 \vec{E} = \mu_0 \mu_r \sigma \frac{\partial \vec{E}}{\partial t} + \mu_0 \mu_r \epsilon_0 \epsilon_r \frac{\partial^2 \vec{E}}{\partial t^2} \tag{2.8}$$

This equation leads to a damped electromagnetic wave inside the medium, which can be described by complex quantities for the susceptibility χ_{el}, the permittivity ϵ_{r} and the refractive index n of the medium. For an isolator the conductivity σ vanishes leading to a real refractive index $n = \sqrt{\mu_r \epsilon_r}$ and a speed of light inside the medium given by $c_{\mathrm{medium}} = c/n$.
With this classical description effects like diffraction and interference are easily explained and for most aspects a semi-classical theory, in which the light is treated classically whereas matter is treated quantum mechanically, is sufficient.

2.1.2 Quantization of the light field

The quantization of the light field is done by introducing the scalar potential ϕ and the vector potential $\vec{A}$ and using the fourier representation of these potentials to obtain the Hamiltonian of the system. From this derivation a few steps will be presented here, while the whole derivation is done elaborately for example in Loudon's book The Quantum Theory of Light [2].
For the vector potential $\vec{A}$ it is also possible to derive a wave equation. As such the vector potential can be expressed as a sum of plane waves, as it is given by

$$\vec{A}(\vec{r},t) = \sum_{\vec{k}} \sum_{\lambda=1,2} \vec{e}_{\vec{k},\lambda} \left(A_{\vec{k},\lambda} \exp\left(-i\omega_{\vec{k}} t + i\vec{k}\vec{r}\right) + A^*_{\vec{k},\lambda} \exp\left(i\omega_{\vec{k}} t - i\vec{k}\vec{r}\right)\right) \tag{2.9}$$

with the wave vector $\vec{k}$ and the two possible polarizations λ. In this the unit vectors of the polarization $\vec{e}_{\vec{k},\lambda}$ are transverse and perpendicular to each other. This leads to the total radiation energy

$$E_{\mathrm{R}} = \sum_{\vec{k}} \sum_{\lambda} \epsilon_0 V \omega^2_{\vec{k}} \left(A_{\vec{k},\lambda} A^*_{\vec{k},\lambda} + A^*_{\vec{k},\lambda} A_{\vec{k},\lambda} \right) . \tag{2.10}$$

Using the conversion from the classical vector potential to the quantum mechanical operators, the Hamiltonian is then given by

$$\hat{H}_{\mathrm{R}} = \sum_{\vec{k}} \sum_{\lambda} \frac{1}{2} \hbar\omega_{\vec{k}} \left(\hat{a}_{\vec{k},\lambda} \hat{a}^\dagger_{\vec{k},\lambda} + \hat{a}^\dagger_{\vec{k},\lambda} \hat{a}_{\vec{k},\lambda} \right) . \tag{2.11}$$

This Hamiltonian resembles the Hamiltonian of an harmonic oscillator expressed in terms of the annihilation operator $\hat{a}$ and the creation operator $\hat{a}^\dagger$:

$$\hat{H} = \hbar\omega \left(\hat{a}^\dagger \hat{a} + \frac{1}{2} \right) . \tag{2.12}$$

Because of that the description of light can be understood by looking at the one dimensional harmonic oscillator. The eigenenergies of the system given by equation 2.12 are $E_{\mathrm{n}} = \hbar\omega \left(n + \frac{1}{2}\right)$. A representation of the eigenstates are the number states $|n\rangle$, which obey the following relations:

$$\hat{a}^\dagger \hat{a} \, |n\rangle = n \, |n\rangle \tag{2.13}$$

$$\hat{a} \, |n\rangle = \sqrt{n} \; |n-1\rangle \tag{2.14}$$

$$\hat{a}^\dagger \, |n\rangle = \sqrt{n+1} \; |n+1\rangle . \tag{2.15}$$

Applying this formalism to the light field n describes the number of excitations with the energy $\hbar\omega$. These quantized excitations of the electromagnetic field are called photons.
With this formalism a beam of light can be considered as a stream of photons. The statistical properties of the photons can differ for different sources of light, which leads to a classification of light as explained in the following section.

2.1.3 Photon statistics

As described in the last section a beam of light can be considered as a stream of photons. Its photon flux Φ is defined as the average number of photons passing through a cross section area A of the beam in one second.

$$\Phi = \frac{I\,A}{\hbar\omega} = \frac{P}{\hbar\omega} \quad ; \quad [\Phi] = \frac{photons}{s} \tag{2.16}$$

In this definition I is the intensity and P the power of the beam. With this the average number of photons in a segment is given by $\overline{n} = \frac{\Phi L}{c}$. The probability of finding n randomly distributed photons in a segment of length L, which is further divided in a large number N of sub segments, is then given by the binomial distribution.

$$P(n) = \frac{N!}{n!\,(N-n)!} \left(\frac{\overline{n}}{N}\right)^n \left(1 - \frac{\overline{n}}{N}\right)^{N-n} \tag{2.17}$$

In the limit of $N \to \infty$ this expression can be written as

$$P(n) = \frac{\overline{n}^n}{n!} \exp\left(-\overline{n}\right) \tag{2.18}$$

As such the statistics of a beam of light with randomly distributed photons is therefore described by a Poissonian distribution. The Poisonian distribution is shown in figure 2.1 for different values of the average photon number $\overline{n}$.

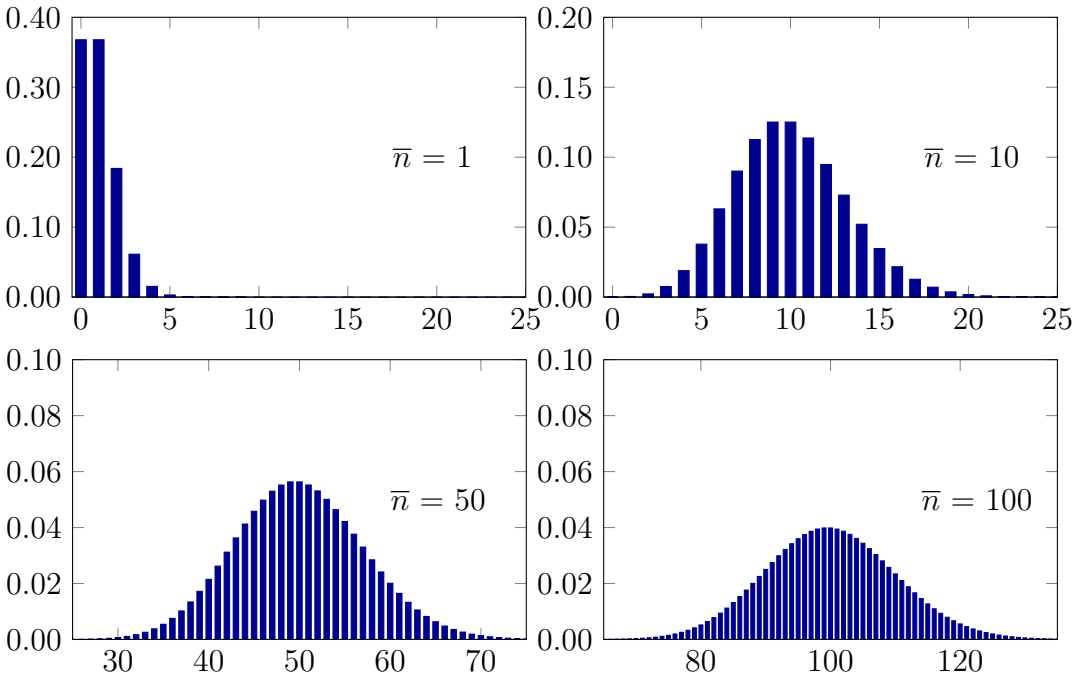

Figure 2.1: Shown is the poissonian distribution for different mean values and as such the probability is plotted against the number of photons. This figure was created on the basis of Fig. 5.3 in [1].

The fluctuation of the photon number around the mean value is characterized in terms of the variance. The variance is defined as the square of the standard deviation Δn. For the Poissonian distribution the variance is given by

$$(\Delta n)^2 = \sum_{n=0}^{\infty} (n - \overline{n})^2 \, P(n) = \overline{n}. \tag{2.19}$$

Accordingly the variance for the Poissonian distribution is equal to its mean value and therefore the standard deviation is $\Delta n = \sqrt{\overline{n}}$. The standard deviation provides a way to classify different types of light. One distinguishes between three different types of light:

- sub-Poissonian statistics: $\Delta n < \sqrt{\overline{n}}$
- Poissonian statistics: $\Delta n = \sqrt{\overline{n}}$
- super-Poissonian statistics: $\Delta n > \sqrt{\overline{n}}$

The difference between the statistical properties of these three types of light is shown in figure 2.2. The figure clearly shows that a sub- / super-Poissonian distribution describes a narrower / broader distribution than the Poissonian distribution.

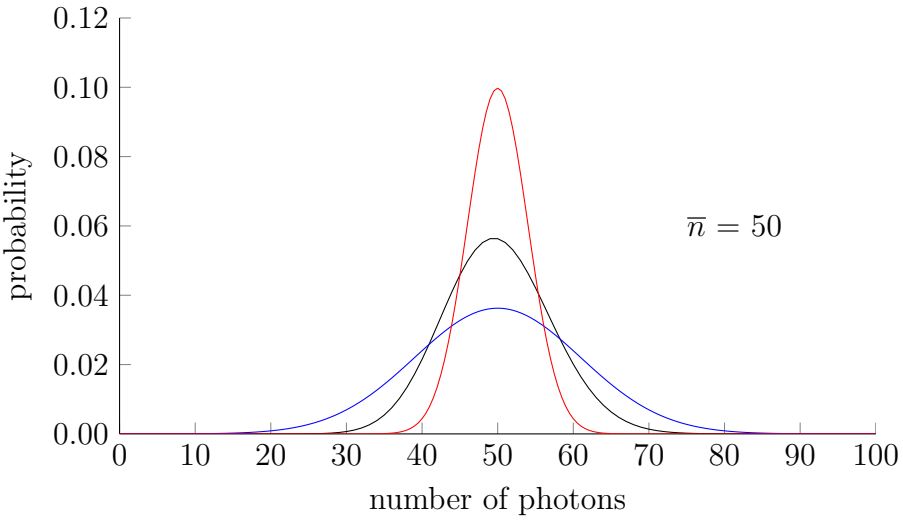

Figure 2.2: Comparison of super- (blue curve), sub- (red) and poissonian distribution (black); based on Fig. 5.4 in [1].

Super-Poissonian statistics are even classically easy to obtain and it is simple to show that a time varying intensity, thermal or chaotic light all lead to the broadening of the probability distribution.
The random distribution of photons described by the poissonian statistics can be obtained from a laser, which emits light coherently. Thereby coherence describes the ability of waves to show stationary interference and is given by the coherence time and length.

Sub-Poissonian statistics however have no classical equivalent, as perfectly coherent light is the most stable form of light in classical optics, showing the least fluctuations. As such the appearance of sub-poissonian statistics is a clear sign for non-classical light. The photon number states $|n\rangle$ possess a fixed value for the photon number n and because of that the standard deviation vanishes. As such the photon number states are the best example for sub-poissonian light.

2.1.4 Photon antibuncing

Alternatively light can also be classified in a different way leading also to a threefold classification[1]. This classification is done by looking at the second-order correlation function $g^{(2)}(\tau)$, defined by

$$g^{(2)}(\tau) = \frac{\langle I(t)\, I(t+\tau)\rangle}{\langle I(t)\rangle\, \langle I(t+\tau)\rangle}\,. \tag{2.20}$$

In this equation the brackets $\langle ...\rangle$ stand for the average over a long period of time. The classification of different types of light is based on the value of $g^{(2)}(\tau = 0)$. With this light can be classified in three different types:

- bunched light: $g^{(2)}(0) > 1$
- coherent light: $g^{(2)}(0) = 1$
- antibunched light: $g^{(2)}(0) < 1$

The correlation function can be measured with an Hanbury Brown-Twiss experiment, which is described in detail in chapter 6 of [1]. A Hanbury Brown-Twiss experiment on the single photon level divides a light beam with a beam-splitter and then measures the photon counts in both paths relative to the other. The time that passes between a photon impact in path 1 and the impact in path 2 is the time τ. For a random distribution of the photons in the beam (coherent light), the impact of the photon in path 2 at each time has the same probability. As such the correlation function, which is normalized, is equal to 1 for every time τ. For bunched light however, the probability of a photon impact for short times is higher and as such the value of $g^{(2)}(0)$ is bigger than 1. A classical equivalent for bunched light can again be easily obtained, for example from a source with a time varying intensity. Non-classical light has a higher order between the photons and as such the probability of an impact for short times decreases. Antibunched light has no classical equivalent and can for example be obtained with a single photon source.

[1]The two classifications are not identical, as sub-poissonian statistics and photon antibunching are not the same manifestation of the same quantum optical phenomenon, as discussed in [13].

2.2 Pulses

This thesis deals with the detection of few-photon light pulses. As such in this section the most important aspects of pulses will be discussed. A pulse is characterized by

- the maximum height,
- the length (normally given by the full width half maximum (FWHM)) and
- the rise / fall time (given by the time a pulse needs to rise from 10% to 90% of its maximum height and accordingly to fall from 90% to 10%)

of the pulse. These characteristics are also illustrated for an arbitrary pulse in figure 2.3.

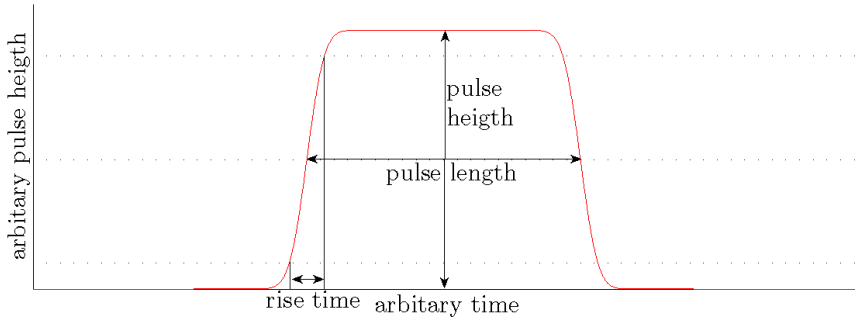

Figure 2.3: Illustration of the height, the length and the rise time of a pulse

To create a light pulse the amplitude of a monochromatic light source has to be modulated. With the process of amplitude modulation new frequency components are added to the signal. The frequency spectrum of a pulse can be obtained by using a fourier transformation. This means, that steeper slopes lead to a broader frequency spectrum.
Considering the propagation of a pulse, each frequency component travels with its respective phase velocity $v_{\mathrm{ph}} = \frac{\omega}{k}$, while the whole pulse travels with the group velocity $v_{\mathrm{g}} = \frac{\partial \omega}{\partial k}$. For light in free space the dispersion relation is given by $\omega = c\,k$ and as such the phase and the group velocity are both equal to the vacuum light speed c. However in dispersive media the velocities can assume different values and the pulse can disperse over time.

2.3 EIT and Slow Light

The following section deals with the effect of electromagnetically induced transparency (EIT) and its application of slow light. This overview of EIT is based on the paper of M. Fleischhauer, A. Imamoglu and J.P. Marangos about EIT: Optics in coherent media [3], with added inputs from [4], [5] and [6].

2.3.1 EIT in a 3-level system

Electromagnetically induced transparency is an effect which renders a 3-level system transparent (or at least improves the transmission) over a narrow spectral range within an absorption line. To achieve this it is necessary to apply two different light fields to two different transitions of the medium as it's shown schematically in figure 2.4 for a Λ-type and a ladder-type system.

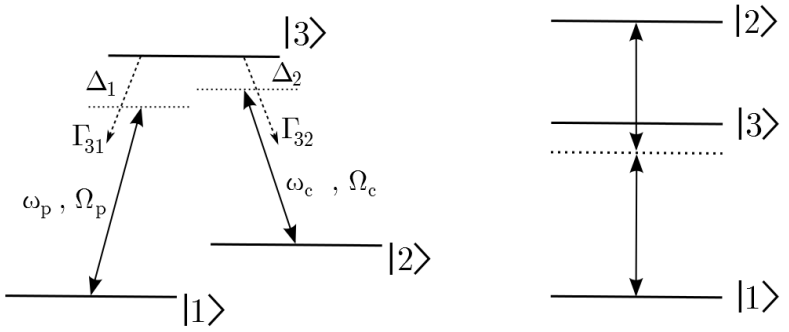

Figure 2.4: Schematic illustration of a 3-level system in which EIT can occur. On the left side a Λ-type system and on the right side a ladder-type system is shown. The Λ-system is labelled with all the important quantities, which are explained in the text.

As shown in figure 2.4 there are 3 levels, for which the transition between the states $|1\rangle$ and $|2\rangle$ is forbidden. The transition between $|1\rangle$ and $|3\rangle$ is driven by the probe laser field with the frequency ω_p. This light field is detuned from the actual transition frequency ω_{31}, with the detuning given by $\Delta_1 = \omega_{31} - \omega_\mathrm{p}$. The second possible transition is driven by the coupling field with the frequency ω_c, with the detuning $\Delta_2 = \omega_{32} - \omega_\mathrm{c}$ from the actual transition. The state $|3\rangle$ has a finite lifetime and decays with the rates Γ_{31} and Γ_{32} to the respective lower states.
The effect of EIT can also be observed in a classical system of springs. In such a system the mass does not move, if it is driven by two sinusoidal forces with the same amplitude but with opposite phases. For a quantum mechanical system this means, that the probability

amplitude of the state $|3\rangle$ has to be driven by two terms of equal magnitude but opposite sign.
Before solving the master equation which leads to the response of the medium, we examine the dressed state picture of the system and the concept of a dark state. The Hamiltonian of the Λ-type system in figure 2.4 is given by $\hat{H} = \hat{H}_0 + \hat{H}_{\text{int}}$, where $\hat{H}_0$ describes the bare atomic states and $\hat{H}_{\text{int}}$ the interaction with both light fields. The interaction Hamiltonian $\hat{H}_{\text{int}} = \vec{\mu}\,\vec{E}$ can be expressed in terms of the Rabi-frequency $\Omega = \frac{1}{\hbar}\,\vec{\mu}\,\vec{E}_0$. In both cases $\vec{\mu}$ describes the electric dipole moment of the transition. Using the rotating wave approximation, in which rapidly oscillating terms of the frequency $\omega_p + \omega_0$ are neglected, the Hamiltonian of the 3-level system can be written as

$$\hat{H} = -\frac{\hbar}{2}\begin{pmatrix} 0 & 0 & \Omega_{\text{p}} \\ 0 & -2\,(\Delta_1 - \Delta_2) & \Omega_{\text{c}} \\ \Omega_{\text{p}} & \Omega_{\text{c}} & -2\,\Delta_1 \end{pmatrix}. \tag{2.21}$$

Diagonalizing the Hamiltonian one obtains $E^0 = 0$ and $E^{\pm} = \frac{\hbar}{2}\left(\Delta_1 \pm \sqrt{\Delta_1^2 + \Omega_{\text{p}}^2 + \Omega_{\text{c}}^2}\right)$ as the eigenvalues and

$$\left|a^+\right\rangle = \sin\Theta\sin\phi\,|1\rangle + \cos\phi\,|3\rangle + \cos\Theta\sin\phi\,|2\rangle \tag{2.22}$$

$$\left|a^0\right\rangle = \cos\Theta\,|1\rangle - \sin\Theta\,|2\rangle \tag{2.23}$$

$$\left|a^-\right\rangle = \sin\Theta\cos\phi\,|1\rangle - \sin\phi\,|3\rangle + \cos\Theta\cos\phi\,|2\rangle \tag{2.24}$$

as the eigenstates. This means that the state $|a^0\rangle$ remains at the same energy, while the states $|a^{\pm}\rangle$ are shifted by the energy $E^{\pm}$. Thereby the eigenstates are expressed in terms of the mixing angles Θ and ϕ, which are in the case of two-photon resonance ($\delta = \Delta_1 - \Delta_2 = 0$) given by

$$\tan\Theta = \frac{\Omega_{\text{p}}}{\Omega_{\text{c}}} \tag{2.25}$$

and

$$\tan 2\,\phi = \frac{\sqrt{\Omega_{\text{p}}^2 + \Omega_{\text{c}}^2}}{\delta_1}\,. \tag{2.26}$$

The state $|a^0\rangle$ has no contribution from the original state $|3\rangle$ and is called a dark state, because there is no possibility of spontaneous emission. For EIT we consider the case of a weak probe field $\Omega_{\text{p}} \ll \Omega_{\text{c}}$. In this case the dark state is identical to the ground state $|1\rangle$ and as such no excitation from this state is possible and as such no radiation from the probe field is absorbed.

The response of a medium[2] to light passing through it can be described by the complex susceptibility $\chi^{(1)}$ of the medium, as mentioned above after the wave equation 2.8 inside a medium. Thereby the imaginary part $\mathrm{Im}\,\chi^{(1)}$ describes the absorption of the medium and the real part $\mathrm{Re}\,\chi^{(1)}$ the dispersion of the medium and as such the refractive index.
In a semiclassical analysis, the light fields will be treated classically with small detunings Δ_1 and Δ_2 compared to their respective Rabi-frequencies Ω_p and Ω_c. The Hamiltonian for the interaction of a 3-level atom with both light fields is

$$\hat{H}_\mathrm{int} = -\frac{\hbar}{2}\left(\Omega_\mathrm{p}(t)\,\hat{\sigma}_{31}\,\mathrm{e}^{i\,\Delta_1\,t} + \Omega_\mathrm{c}(t)\,\hat{\sigma}_{32}\,\mathrm{e}^{i\,\Delta_2\,t} + h.c.\right), \tag{2.27}$$

where $\hat{\sigma}_{ij} = |i\rangle\langle j|$ is the atomic projection operator and $h.c.$ means the hermitian conjugate of the first two terms in the brackets. This Hamiltonian can also be obtained from a fully quantized analysis and is equivalent to the earlier used interaction Hamiltonian.
The quantum mechanical treatment of the 3-level system is done in the density-matrix formalism. Involving damping terms in the von-Neumann equation we obtain the following master equation for the dynamics of the system:

$$\begin{aligned}\frac{d\rho}{dt} = \frac{1}{i\hbar}\left[\hat{H}_\mathrm{int},\rho\right] &+ \frac{\Gamma_{31}}{2}\left(2\,\hat{\sigma}_{13}\rho\hat{\sigma}_{31} - \hat{\sigma}_{33}\rho - \rho\hat{\sigma}_{33}\right)\\ &+ \frac{\Gamma_{32}}{2}\left(2\,\hat{\sigma}_{23}\rho\hat{\sigma}_{32} - \hat{\sigma}_{33}\rho - \rho\hat{\sigma}_{33}\right)\\ &+ \frac{\gamma_{2\mathrm{deph}}}{2}\left(2\,\hat{\sigma}_{22}\rho\hat{\sigma}_{22} - \hat{\sigma}_{22}\rho - \rho\hat{\sigma}_{22}\right)\\ &+ \frac{\gamma_{3\mathrm{deph}}}{2}\left(2\,\hat{\sigma}_{33}\rho\hat{\sigma}_{33} - \hat{\sigma}_{33}\rho - \rho\hat{\sigma}_{33}\right)\end{aligned} \tag{2.28}$$

In this equation the two terms following the commutator describe the spontaneous emission, while the last two terms describe energy conserving dephasing processes, such as decays in states not included in the 3-level system. The rates describing the dephasing and decay rates can be combined to $\gamma_{31} = \Gamma_{31} + \Gamma_{32} + \gamma_{3\mathrm{deph}}$ and $\gamma_{32} = \Gamma_{31} + \Gamma_{32} + \gamma_{3\mathrm{deph}} + \gamma_{2\mathrm{deph}}$.
Using $\rho_{11} \approx 1$ and the rotating wave approximation, the master equation can be solved to obtain the linear susceptibility.

$$\begin{aligned}\chi^{(1)}(\omega_\mathrm{p}) = \frac{|\mu_{13}|^2\,\varrho}{\epsilon_0\,\hbar}\cdot\Bigg(&\frac{4\,\delta\left(|\Omega_\mathrm{c}|^2 - 4\,\delta\,\Delta_1\right) - 4\,\Delta_1\,\gamma_{2\mathrm{deph}}^2}{\left||\Omega_\mathrm{c}|^2 + \left(\gamma_{31} + 2\,i\Delta_1\right)\left(\gamma_{2\mathrm{deph}} + 2\,i\delta\right)\right|^2}\\ &+\; i\,\frac{8\,\delta^2\,\gamma_{31} + 2\,\gamma_{2\mathrm{deph}}\left(|\Omega_\mathrm{c}|^2 + \gamma_{2\mathrm{deph}}\,\gamma_{31}\right)}{\left||\Omega_\mathrm{c}|^2 + \left(\gamma_{31} + 2\,i\Delta_1\right)\left(\gamma_{2\mathrm{deph}} + 2\,i\delta\right)\right|^2}\Bigg)\end{aligned} \tag{2.29}$$

In this equation $\delta = \Delta_1 - \Delta_2$ is the two-photon detuning. In the case of two-photon resonance $\delta = 0$ the imaginary part of $\chi^{(1)}$ vanishes (for $\gamma_{2\mathrm{deph}}$) and as such the there is no absorption.

[2]Here only a linear medium is considered and as such only the first order susceptibility is important. For nonlinear effects which can also be achieved with EIT higher orders of the susceptibility have to be considered.

The real and imaginary parts of $\chi^{(1)}$ are shown in figure 2.5. As shown there is a narrow transmission window inside the absorption valley. In the same spectral range there is a steep dispersion (see in the figure for $\mathrm{Re}\,\chi^{(1)}$), which leads to the effect of slow light that will be discussed in the next section.

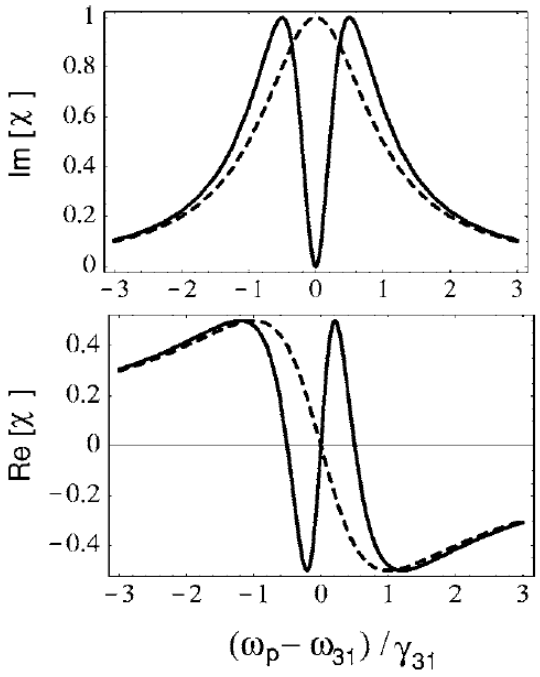

Figure 2.5: Linear susceptibility as a function of the detuning $\delta = \omega_\mathrm{p} - \omega_{31}$ for a 2-level system (dashed line) and a 3-level system (solid line). The upper figure shown the imaginary part of the susceptibility, which describes the absorption and the lower picture shows the real part which determines the refractive index. Taken from FIG. 1 in [3]

In actual systems (especially dense vapours) the dephasing rate $\gamma_{2\mathrm{deph}}$ does not vanish, due to collisions between the atoms (in a vapour cell also with the wall), to the spectral linewidth of the lasers and also due to electric or magnetic fields. In such systems EIT is also observable, as long as $|\Omega_\mathrm{c}|^2 \gg \gamma_{31}\,\gamma_{2\mathrm{deph}}$. Because of the dephasing the transmission is no longer perfect and for $\gamma_{2\mathrm{deph}} \gg \gamma_{31}$ the transmission window vanishes completely. As such EIT is also observable in hot atomic gases. The Doppler broadening in such a system in a Λ-configuration has no adverse effect on the EIT, as long as copropagating laser beams are used. This is because the energy shift caused by the movement of the atoms similarly changes both detunings and as such maintains the two-photon detuning. For counterpropagating beams the susceptibility has to be integrated over the velocity distribution of the atoms. This argument is reversed for a ladder-type system

In an optically thick medium the important quantity is the amplitude transfer function

$$T(\omega_\mathrm{p}, z) = \exp\left(ik\,z\,\frac{\chi^{(1)}}{2}\right). \tag{2.30}$$

In this $k = \frac{2\pi}{\lambda}$ is the wave number and z the length of the medium. Near the resonance ($\delta = 0$) the spectrum is given by a gaussian profile with the width $\Delta\omega_\mathrm{trans}$ given in the following equation.

$$\Delta\omega_\mathrm{trans} = \frac{\Omega_\mathrm{c}^2}{\sqrt{\Gamma_{31}\,\gamma_{31}}}\,\frac{1}{\sqrt{\varrho\,\sigma\,z}} \qquad (\varrho\,\sigma\,z \gg 1) \tag{2.31}$$

In this equation $\sigma = \frac{3\,\lambda^2}{2\pi}$ is the absorption cross section of a atom and ϱ the density of the atoms.

2.3.2 Slow Light

As seen in figure 2.5 the real part of the susceptibility $\chi^{(1)}$ depends linearly on the frequency close to the two-photon resonance $\delta = 0$. For a vanishing dephasing γ_2deph the real part can be approximated by

$$\mathrm{Re}\,\chi^{(1)} = \eta\,\frac{2\,\Gamma_{31}}{\Omega_\mathrm{c}^2}\,\delta\, + \mathcal{O}(\delta^2) \tag{2.32}$$

in which $\eta = \frac{3}{4\pi^2}\,\varrho\,\lambda^3$. The group velocity of a light pulse in a medium with a varying refractive index $n(\omega)$ is given by

$$v_\mathrm{g} = \left.\frac{d\omega_\mathrm{p}}{dk_\mathrm{p}}\right|_{\delta=0} = \frac{c}{n + \omega_\mathrm{p}\,\frac{dn}{d\omega_\mathrm{p}}}. \tag{2.33}$$

Since the linear dispersion is positive near the two-photon resonance, this leads to a reduction of the group velocity in the medium. At the same time the absorption of the medium vanishes (or at leasts decreases) and as such light can be transmitted through the medium. The decreased group velocity leads to a delay inside of a medium with the length L. The delay is given by

$$\tau_\mathrm{d} = L\left(\frac{1}{v_\mathrm{g}} - \frac{1}{c}\right) = \varrho\,\sigma\,L\,\frac{\Gamma_{31}}{\Omega_\mathrm{c}^2}. \tag{2.34}$$

The last equality is only valid for single-photon resonance ($\Delta_1 = 0$). For $\Delta_1 = 0$ the second-order term in equation 2.32 vanishes exactly and as such there is no group velocity dispersion. With this a pulse travelling through the medium maintains its shape. The dephasing γ_2deph leads to a change in the denominator of the equation from Ω_c^2 to $\Omega_\mathrm{c}^2 + \gamma_{31}\,\gamma_\mathrm{2deph}$ and as such to a smaller delay.

As a light pulse enters a medium which shows EIT, the pulse becomes spatially compressed (in the direction of propagation), because the speed of light inside the medium is much smaller than on the outside. The reverse occurs when the pulse leaves the medium. The strength of the electric field during this compression however remains the same. Considering the slow light propagation from the point of view of the atoms, the effect can be understood as the storing of energy from the light field inside the medium and the coupling field. As such the process can be considered as a stimulated Raman adiabative return. At the beginning the atoms are all in the dark-state $|1\rangle$ due to the optical pumping due to the coupling field. This dark-state is changed to a superposition of $|1\rangle$ and $|2\rangle$ when the front end of the probe pulse reaches the medium. This change of the dark-state takes energy out of the pulse and stores it in the coupling field and the atoms. When the pulse reaches its maximum value, the process is reversed and the energy is returned into the pulse. The change of the dark-state depends on the strength of the coupling field and the larger the change of the dark-state (done with a weaker coupling field), the longer the delay of the pulse.
This can also be understood by considering the propagation of polaritons, which describe a coherent mixture of electromagnetic and atomic spin excitation. There are two polaritons, the dark (Ψ) and the bright (Φ) polarition, which are defined in the equations 2.35 and 2.36. The mixing angle between dark and bright polariton is given by $\tan^2\theta = \frac{\varrho\,\sigma\,c\Gamma_{31}}{\Omega_c^2}$.

$$\Psi(z,t) = \cos\theta\,\mathcal{E}_p(z,t) - \sin\theta\,\sqrt{\varrho}\rho_{21}(z,t)\,\mathrm{e}^{i\Delta k\,z} \tag{2.35}$$

$$\Phi(z,t) = \sin\theta\,\mathcal{E}_p(z,t) + \cos\theta\,\sqrt{\varrho}\rho_{21}(z,t)\,\mathrm{e}^{i\Delta k\,z} \tag{2.36}$$

In this equation $\mathcal{E}_p(z,t)$ is the normalized probe field strength which is related to the electric field by $E_p = \mathcal{E}_p\sqrt{\hbar\omega/2\epsilon_0}$ and Δk is the difference between the wave vectors of the probe and coupling beam in the direction of propagation. For a strong coupling field (mixing angle $\theta \to 0$), the dark state polariton is almost electromagnetic in its nature and as such there is only a small slowdown. For a weaker coupling field ($\theta \to \pi/2$) the dark-state polariton has the character of a spin-excitation, which corresponds to a vanishing velocity. As such the effect of slow light can be understood using the propagation of the dark-state polaritons.
The limitations of slow light can be discussed by considering the ratio between delay time τ_d and pulse length τ_p. An upper limit of this value is given due to the finite lifetime of the dark resonance. Another upper limit for the ratio is given by the opacity $\varrho\,\sigma L$ of the medium:

$$\frac{\tau_\mathrm{d}}{\tau_\mathrm{p}} \ll \sqrt{\varrho\,\sigma L}. \tag{2.37}$$

As such it is necessary to have an optically thick medium (which relates to an high opacity) to achieve a noticeable delay. Another important aspect is the spectral width of the pulse, because even for perfect conditions nonresonant frequencies are absorbed.

2.3.3 Rubidium D_2 Line

In the measurements done in the advanced laboratory experiment[3] a Rubidium vapour cell was used. In this vapour cell the D_2-line of Rubidium was used to achieve a 3-level system, which shows EIT. Rubidium has two stable isotopes (^{85}Rb and ^{87}Rb) which were both present in the used vapour. The level scheme of the D_2-line is shown in figure 2.6 for both isotopes.

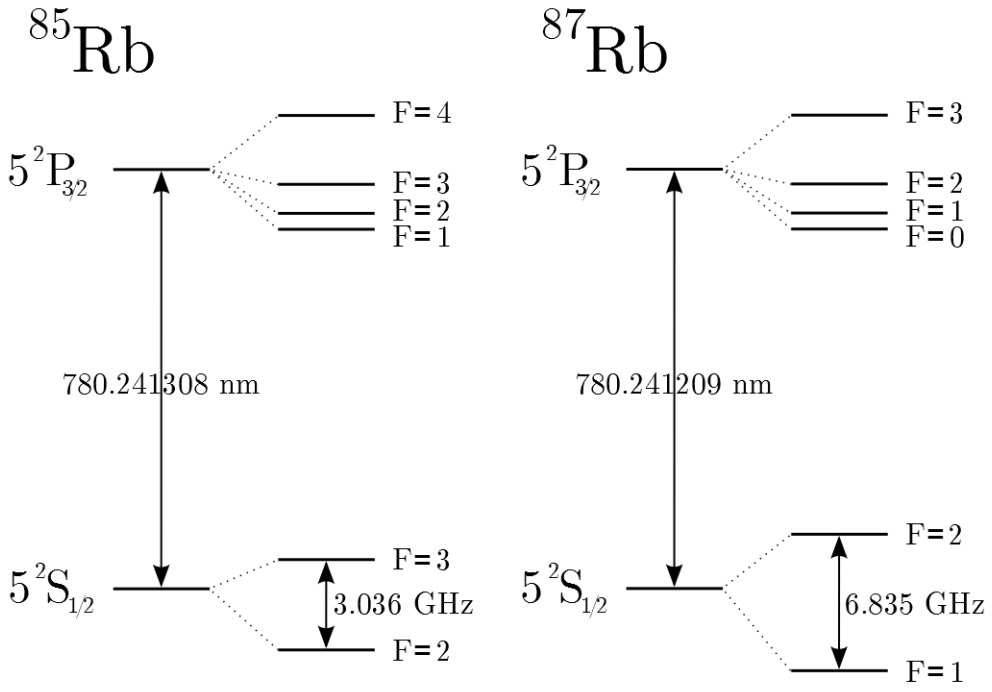

Figure 2.6: Level system of the Rubidium D_2 line. On the left side the level system of ^{85}Rb is shown[7] and on the right side of ^{87}Rb [8].

Due to this level schema the absorption spectrum shows four valleys, from which the middle two are due to the ^{85}Rb and the two outward lines are due to the ^{87}Rb. It is possible to realize a Λ-type 3-level system with the two hyperfine S-states, while the upper level can be any of the hyperfine P-states.

[3]Fortgeschrittenen Praktikum, Versuch EIT

2.3.4 Rydberg EIT

EIT can also be observed in a ladder-type system, in which the upper state corresponds to a Rydberg-state.

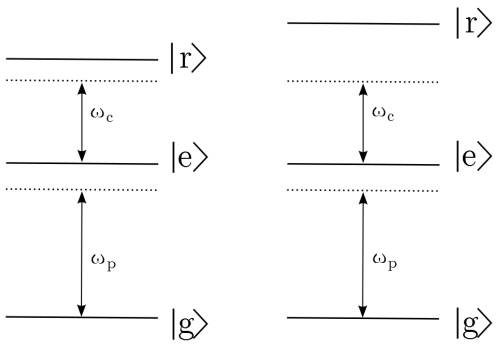

Figure 2.7: Level system of the Rydberg EIT. On the left side system for a single photon, showing EIT. On the right side the interaction between two Rydberg states shifts the coupling transition out of resonance and the EIT vanishes.

For small optical densities this system acts as a normal ladder-type system showing EIT. The strong interaction between Rydberg states (Van der Waals force) suppresses multiple excitations in a blockade Volume (Rydberg blockade). For high optical densities per blockade volume the blockade effect leads to different properties of the system. For a single probe photon the coupling field leads to EIT and the photon can pass through the medium. For a second photon however the interaction between the Rydberg states shifts the coupling transition out of resonance and the second photon effectively sees a 2-level system, which leads to absorption. As such the system shows absorption for photon pairs, while it's transparent for single photons.
In the experiment the ground state $|g\rangle$ is the ground state of ^{87}Rb, which is the $5\,S_{1/2}$ state. As excited state $|e\rangle$ the $5\,P_{3/2}$ was used and for the Rydberg state the $40\,S$-state. The blue coupling laser was stabilized to be resonant to the transition between the excited state and the used Rydberg state with a frequency of 623.3724 THz.

3 Experimental Setup

In this chapter the devices and programs used for the measurements performed during this thesis will be presented and briefly explained.

3.1 Single Photon Counting Module

The aim of this thesis was to work with and test the single photon counting modules (SPCM), that are to be used in the experiment of the Rydberg Quantum Optics group. These modules are two COUNT-250C-FC single photon counter from LASER COMPONENTS, one of which is shown in figure 3.1.

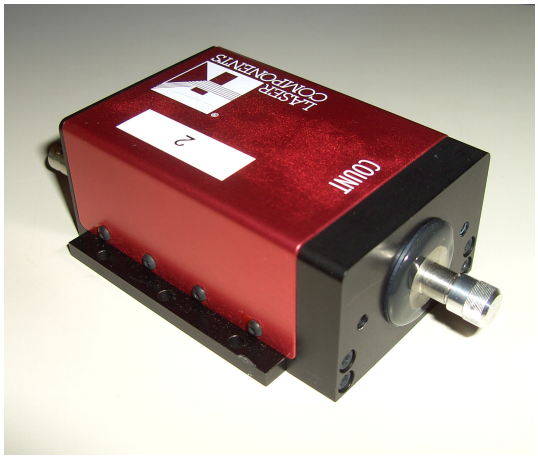

Figure 3.1: Picture of the used Single Photon Counting Module from Laser Components

These single photon counters are based on a silicon avalanche photodiode. A photodiode is simply a semiconductor diode in reverse direction, which uses the inner photoelectric effect to create a current if light falls on it. A single photon creates an electron-hole-pair, which by itself is not enough to be measured. In an avalanche photodiode this single electron-hole-pair is multiplied through impact ionization (avalanche effect) by applying a high voltage. With this weak light signals down to single photons can be detected.

The used single photon counting modules create a TTL-output pulse of 25 ns[4] length with a delay of 50 ns between the photon impact and the output pulse. The avalanche photodiode inside these modules is sensitive in a spectral range from 400 nm to 1000 nm, with its efficiency maximum of approximately 70% in the red spectral region. The two modules which were used during this thesis vary in some of their important quantities and as such the most important properties of the two modules are compared to each other in the following table.

[4] All of the values are taken from the data sheet of the COUNT-250C series [9]

	SPCM 1	SPCM 2
serial number	C2621	D2642
dead time	56 ns	55 ns
dark count rate	130 $\frac{1}{s}$	202 $\frac{1}{s}$
efficiency @ 670 nm	84%	87%
efficiency @ 810 nm	54%	56%

Table 3.1: Comparison of the two single photon counting modules as specified by Laser Components [9]

The counting modules can be turned on and off with a gating function. This gating has a response time of typically 20 ns for turning the module off and a response time of typically 85 ns for turning it on. Another important aspect is the maximal count rate of 5 Mio. counts/s and the necessary correction factor for high counting rates, caused due to the dead time of the photodiode. The true counting rate R_{actual} can be calculated from the measured rate R_{measured} by the following equation:

$$R_{\text{actual}} = \frac{R_{\text{measured}}}{1 - R_{\text{measured}} \cdot T_{\text{dead}}} \tag{3.1}$$

3.2 FPGA Time-Tagger

For the high resolution timing of the TTL-pulses emitted by the counting modules a field-programmable gate array (FPGA) based Time-Tagger was used, which was developed in the group of Dr. H. Fedder in the 3rd physical institute. This FPGA based Time-Tagger can count on up to 8 independent channels with a time resolution of 60 ps.

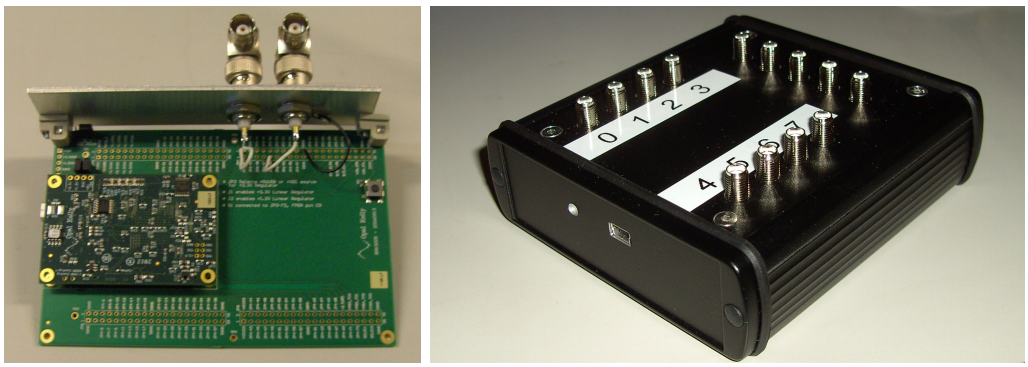

Figure 3.2: Picture of the prototype version (left) and the final version (right) of the FPGA Time-Tagger

The control programs of the Time-Tagger were also developed in the 3rd institute. The control of the measurements with the Time-Tagger is done in the programming language

Python. During this thesis the control programs were developed further by Hannes Gorniaczyk, mainly to work together with the experimental control system of the RQO experiment.
For the measurements done during this thesis, two different counting functions of the device were used:

- A function that counts all pulses on each individual channel and displays the counts per second averaged over the time since the start command (or since the last clear command).
- A pulsed function that counts the incoming pulses in a specified time (bin width) for a specified number of bins, after a trigger pulse (the rising slope of the pulse) is detected on a different channel. This function displays the counts of each bin in a two dimensional array. A second trigger pulse starts the measurement again and the counts after the second trigger are added to the previous counts in the respective bin. There can also be specified a number of repetitions (shots), so that the counts after a new trigger pulse are written in a new line. The output of this mode is then a (number of shots)×(number of bins) matrix.

The principle behind the pulsed measurement is also shown in figure 3.3.

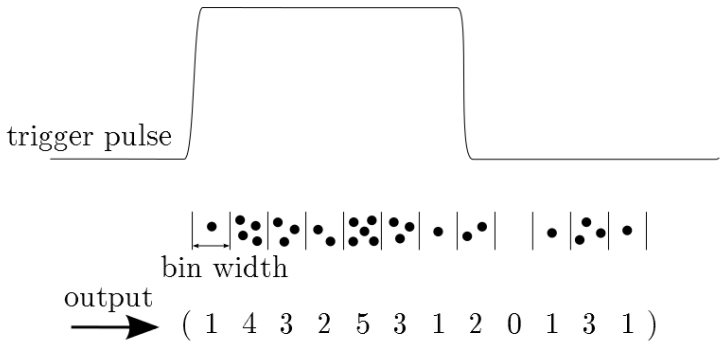

Figure 3.3: Illustration of the pulsed measurement mode of the Time-Tagger, with the trigger pulse, the bins filled with photons (representing the TTL-pulses measured during the time of the bin) and the output array.

3.3 Pulseblaster Board

To create the pulses a Pulseblaster PCI board from SpinCore was used. With this board it is possible to create short electrical pulses down to a length of 2 ns. The control software, the implementation and the testing of this device was done by Udo Hermann as a bachelor thesis a year earlier. Further information about the Pulseblaster board can be found in [10].

3.4 Acoustooptic Modulator (AOM)

To create the light pulses an acoustooptic modulator (AOM) was used. The basic principle of an AOM is the interaction between a light beam and a density modulation inside of a medium. The density modulation is caused by an acoustic wave, which is created with a piezoelectric transducer. This density modulation leads to a similarly changing refractive index of the medium. The speed of the acoustic oscillation is much slower than the oscillation of the light and because of that the light sees a 'frozen' modulation of the refractive index, which corresponds to a diffraction grating. The principle of the AOM is also illustrated in figure 3.4.

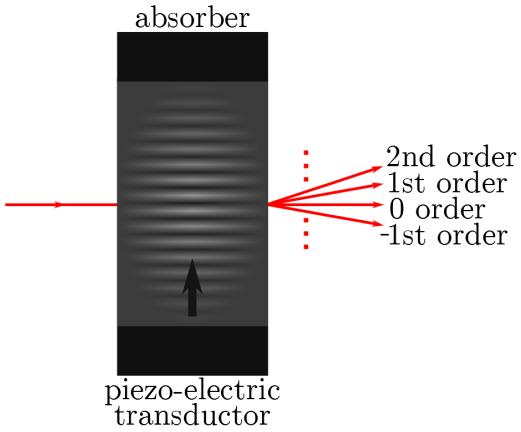

Figure 3.4: Basic principle of an AOM: The incoming light beam interacts with the acoustic wave, which acts as a diffraction grating. The light coming out of the AOM is split into different orders, with different angles.

Using the 1st-order of the light after the AOM it is possible to create light pulses by turning on and off the piezoelectric transducer which generates the sound waves in the quartz crystal. To turn the piezoelectric transducer on and off short electric pulses are needed, which were created with a Pulseblaster board.

4 Measurements

In this chapter the measurements done during this thesis are presented, beginning from the testing of the new SPCMs and the new Time-Tagger and ending with the delay measurement of the RQO experiment.

4.1 Dark Counts and Time-Tagger

At the beginning of this thesis the single photon counting modules were tested. After testing the functionality and the gating function, the dark count rate was measured and compared to the specified value. This measurements was used to test the functionality of the new Time-Tagger. For this measurement the light input of the SPCM was closed and the counts of the SPCM recorded for a duration of 45 minutes using the pulsed feature of the Time-Tagger with a single trigger pulse. The result of this measurement is shown in figure 4.1. Evaluating the mean value of the recorded data, we get the following dark count rates:

- SPCM1: 128 counts/s
- SPCM2: 200 counts/s

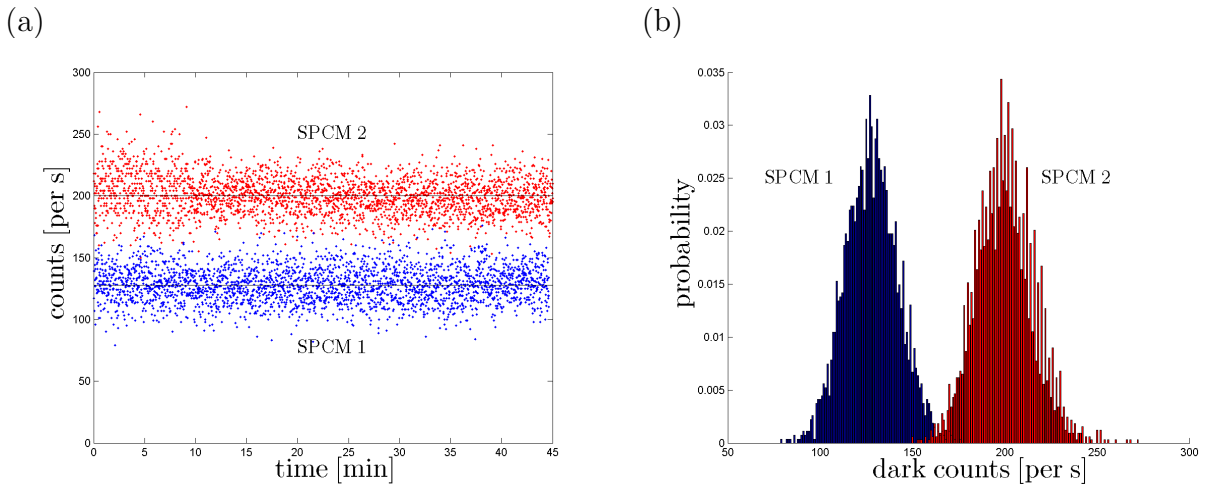

Figure 4.1: Dark count rate of the two SPCM (a) and histogram of the dark counts (b)

These values for the dark count rate agree with the specified values, given in table 3.1, with both measured values being slightly smaller. Plotting the recorded dark counts in a

histogram, shows a poissonian distribution (compare figure 4.1 (b)). This is as expected for the random process of Generation-Recombination noise of a semiconductor device.

After proving the functionality of the measurements done with the Time-Tagger, which was only a prototype version in the beginning of this thesis, light was actually measured. In these measurements an oscillation of the measured counts was observed (as seen in figure 4.2 (a)) when the voltage of the trigger channel was changed (in the figure due to the incoming trigger pulse). This leads to the assumption that the oscillation was caused by cross talk between the two channels. The left side of figure 4.2 shows the oscillation at the beginning of a measurement of the fall time of a light pulse created with an AOM. The observed oscillation shows a period of about 6 ns and changed its direction when the used channels were flipped.

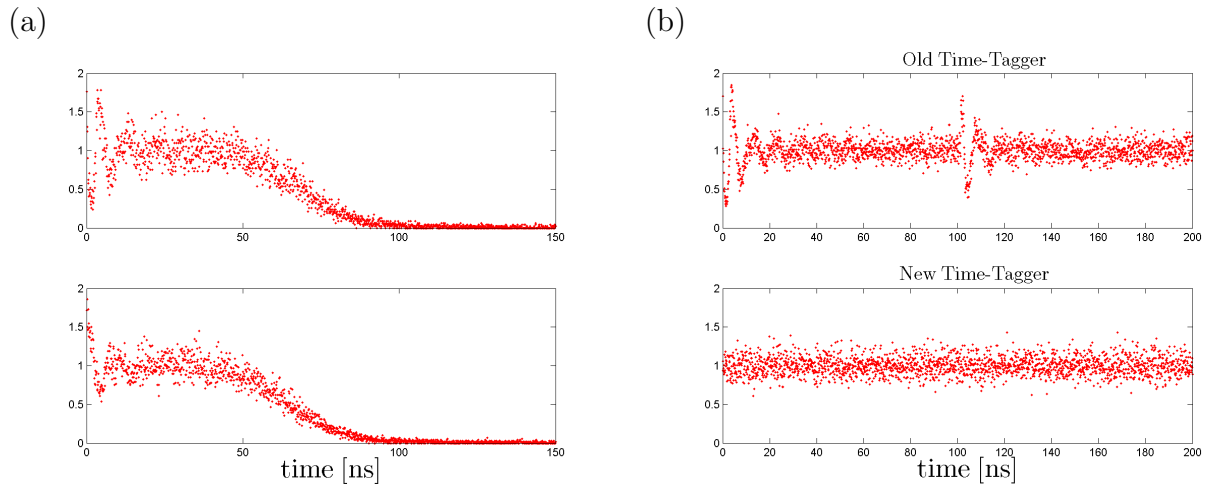

Figure 4.2: Left: Oscillation of the recorded counting rate, which was normalized by the mean value and oscialltion with flipped channels. Right: A comparison of the old and new Time-Tagger shows that the oscillation doesn't show on the new version.

Later in the thesis a new version of the Time-Tagger was used, for which the oscillation did not show. Figure 4.2 (b) shows a comparison of the old and the new Time-Tagger, the old showing an oscillation while the new one doesn't.

4.2 Photon Statistics of Laser Light

As next step the statistics of laser light was investigated. For this measurement the beam of a diode laser was sent through an optical isolator and then though an AOM, after which the first order light was coupled it into a fiber connected to the SPCM. The recorded data was then multiplied with the correction factor (as given by equation 3.1) and then plotted in a histogram as shown in figure 4.3.

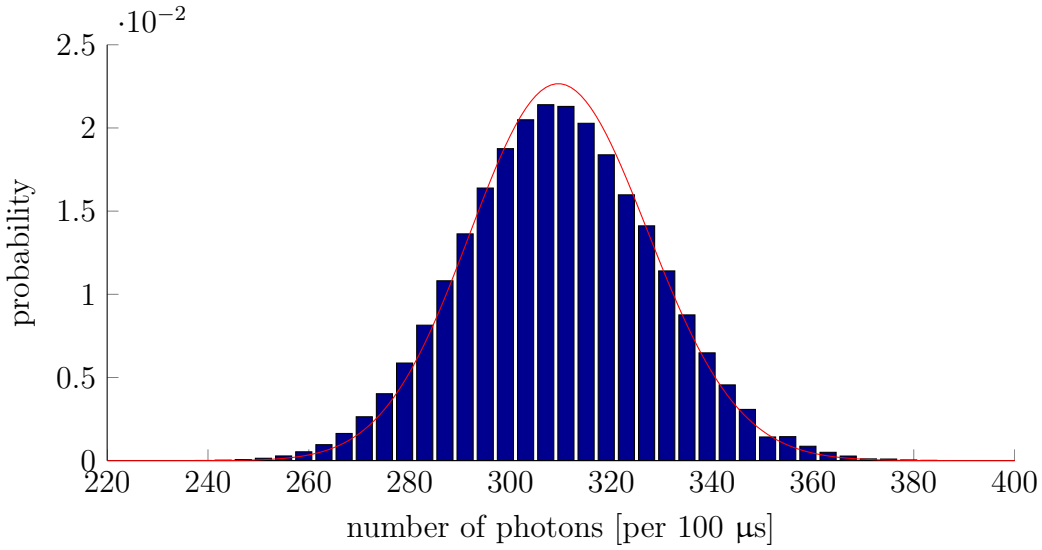

Figure 4.3: Histogram of the photon number detected in a time interval of 100 µs compared to an poissonian distribution with the same mean value.

As explained in the theory, coherent laser light should show a poissonian distribution in the number of photons. Using this knowledge a poissonian distribution, with its mean value given by the data, was plotted in the same figure. As seen in the plot the data and the poissonian distribution do not agree perfectly. Evaluating the variance of the data we receive a higher value than the mean value. Dividing the calculated variance through the mean value we get a factor of 1.1726.

This means the measurements done are not shot noise restricted as already a higher deviation was detected as there should be for coherent light. The added noise could come from the laser itself, as the used laser was not stabilized. This was checked by measuring the statistics of another laser (the laser used in the slow light measurements done in the advanced laboratory). For this laser there was also more than shot noise present, but the ratio between the variance and the mean value was decreased to 1.1061.

The added noise detected for both laser sources could be caused by different factors. It could be caused from fluctuations in the power supply of the diode lasers or even from the coupling of the the light into a fiber. Another reason for the noise could be the AOM in the path of the light.

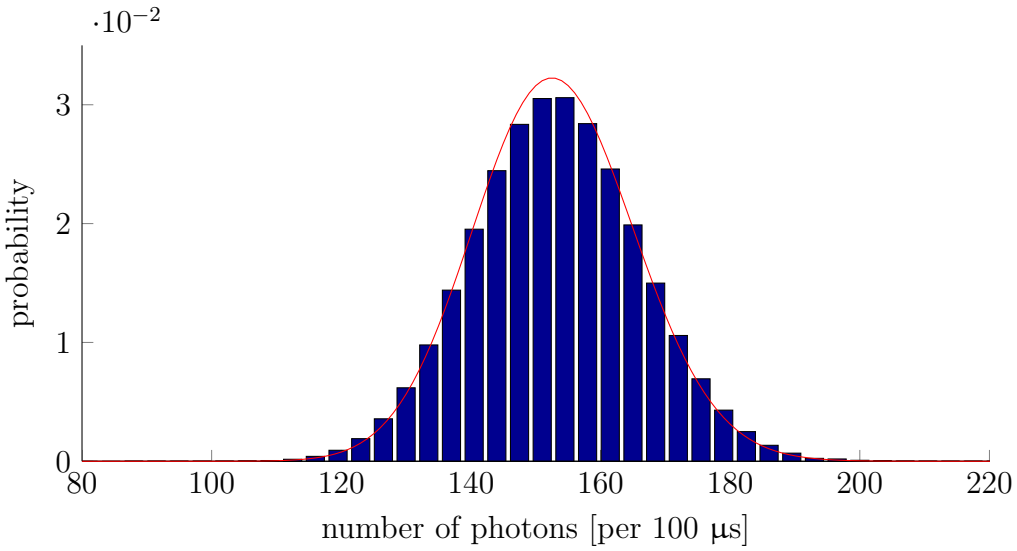

Figure 4.4: Photon statistics recorded for a different laser.

4.3 Classification of a Mechanical Shutter

After proving the functionality of the measurements done with the SPCMs and the Time-Tagger, light pulses created with a mechanical shutter were examined as a first application. The shutter consists of a small movable metal plate, which can take two different positions, changing the position due to magnetic forces if the TTL-input is changed. In the experiments mechanical shutter are used to avoid as much stray light as possible and as such the reliability of the shutter was investigated.

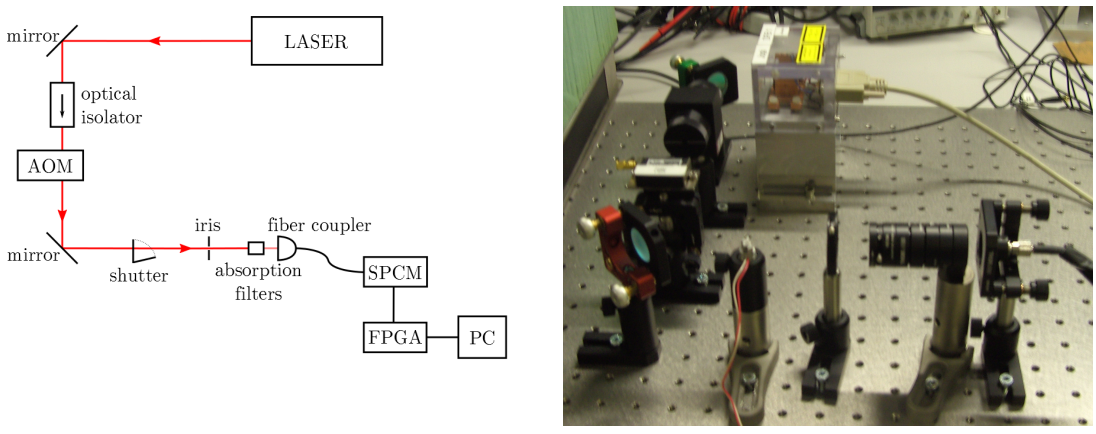

Figure 4.5: On the left side the schematic setup for the shutter measurements and on the right a photo of the actual setup is shown.

For the measurements the setup was build as shown in figure 4.5. As light source a diode laser with a wavelength of 780 nm was used. The beam was then sent through an optical isolator, which prevents reflections going back into the laser. After the isolator the beam passed through an AOM, after which the first order of light was used (This was done to be able to compare the measurements to later measurements in which the pulses were created with an AOM). With a mirror the beam was then coupled into a fiber. In the path of the light from mirror to fiber the shutter was placed. For the exact positioning of the shutter it was looked to it that the metal plate was roughly orthogonal to the beam. This was done because the initial position has a great effect on both the rise and the fall time of the created light pulses. Most measurements were done without focusing the laser, leading to a beam waist of roughly 1 mm, which corresponds to nearly the whole metal plate filled with light. Later a lens was placed before the shutter to focus the laser at the position of the shutter, as it's done in most experimental setups. After the shutter the beam was collimated again and an iris was used to block the other orders of the light created by the AOM. Optical absorption filters were placed in the optical path to attenuate the beam of light down to the low photon count rates needed for the SPCM. The fiber was connected to the SPCM from which the output went to the Time-Tagger and its controlling software. The whole setup was placed inside of a casing of carton to minimize the effect of the surrounding light.
As mentioned above absorption filters were needed to attenuate the beam to the few-photon level. To obtain a counting rate of 1 Mio counts/s, a 100 mW laser beam has to be attenuated with a factor of roughly 10^{-12}, as calculated in the following following equation for an unit time.

$$P = n \frac{h\,c}{\lambda} = 2.55 \cdot 10^{-13}\,\mathrm{W} \tag{4.1}$$

$$\rightarrow \frac{P}{P_{\mathrm{laser}}} = 2.55 \cdot 10^{-12} \tag{4.2}$$

To be on the safe side and because the absorption filters each have a percentage error in their optical densities, more filters were used in the beginning and then reduced until the desired counting rate was achieved.
Before the SPCM was used, the delay between electric signal and light pulse was measured using a photodiode and fewer absorption filters. Those delay measurements are given for the rising and the falling slope of the light pulse in figure 4.6 (a) and (b). The blue curve is the electrical TTL-signal and the red curve is the measured voltage of the photodiode created due to the light pulse. Both curves were normalized to easier obtain the rise/fall time.

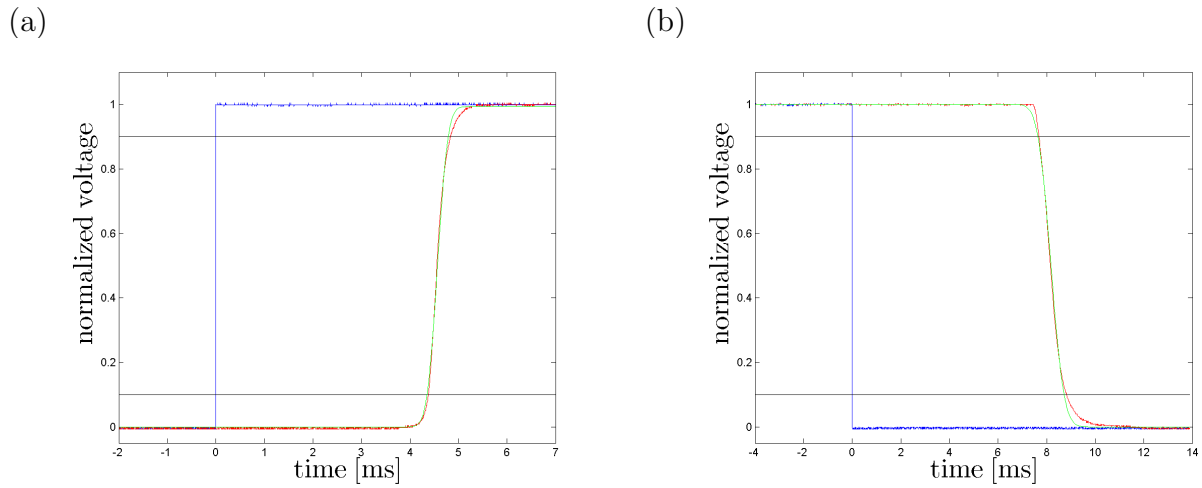

Figure 4.6: Rising and falling slope of the shutter pulse measured with the photodiode with a fitting curve each and compared to the electric signal to determine the delay.

The delay of the rising slope was measured to $\Delta t_{\text{Open}} = 4.37\,\text{ms}$ and the delay of the falling slope to $\Delta t_{\text{Close}} = 8\,\text{ms}$. These times were later used in the SPCM measurements to reduce the measurement to the region of interest. Also seen in the figure is a fitting curve[5] using the error function. The error function is the integral over a gaussian function, corresponding in the measurement to a constant opening/closing shutter and a gaussian profile of the laser. Both requirements weren't completely fulfilled in the experiment, but as seen in the figure the approximation is already quite good.
The rise and the fall time of the pulse were taken from the fitting curve as the times between 10% and 90% of the pulse height, indicated by the black lines in the figure. The obtained values are 0.45 ms for the rise time and 1.15 ms for the fall time.
The SPCM and the Time-Tagger was then used to reconstruct an 1 second light pulse after many measurements each detecting only a few photons per 100 µs bin. Calculating the mean value of each bin and normalizing it to counts per second the light pulse is shown in figure 4.7.

[5]For the rising slope a function of the form $p_1\left(1+\text{erf}(\frac{t-p_2}{p_3})\right)$ and for the falling slope of the form $p_1\left(1-\text{erf}(\frac{t-p_2}{p_3})\right)$ was used, in which the p_i are the parameters.

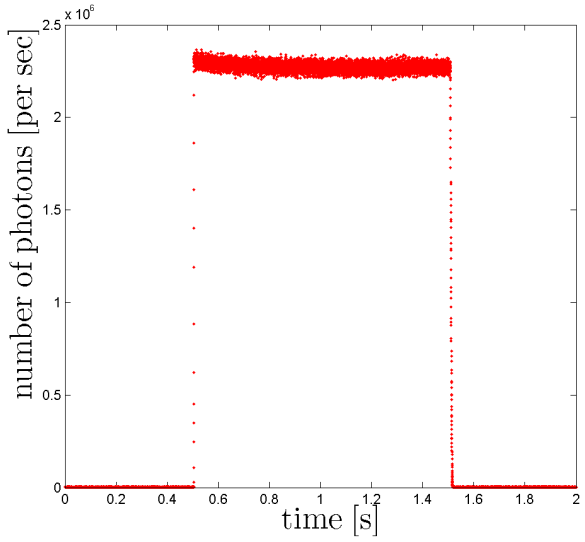

Figure 4.7: Reconstruction of a one second light pulse created with an mechanical shutter.

Measurements of the pulse with a better time resolution (bin width of 1 µs) were done to determine the rise and fall time of the light pulse. As shown in figure 4.8 an error function was fitted to the data, which was normalized to the counting rate of an open shutter, in order to obtain the rise and fall time.

(a) (b)

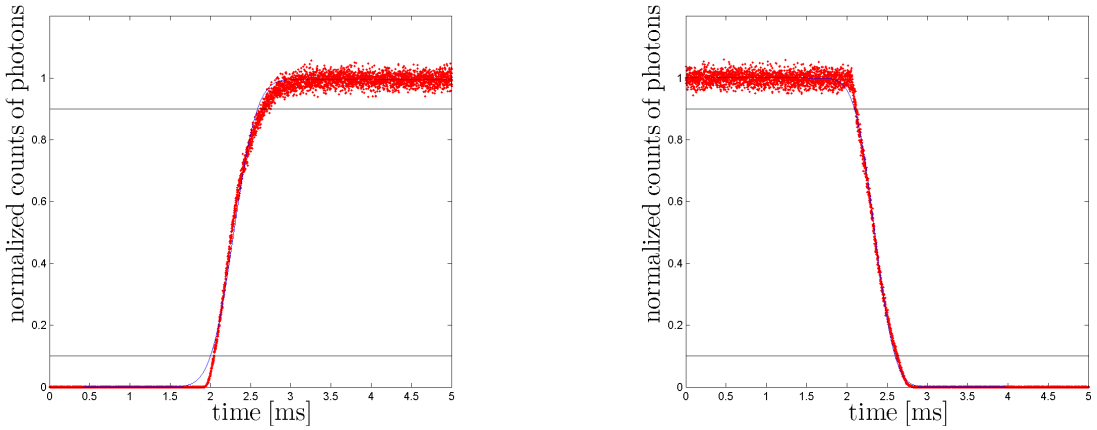

Figure 4.8: Rising and falling slope of a light pulse created by a shutter, measured with the SPCM.

From the figure the rise time was taken to be 0.586 ms and the fall time to be 0.505 ms. These obtained times vary from the ones measured with the photodiode. This could be due to small changes in the position of the shutter caused during the modification of the setup or else due to mechanical oscillations caused by the shutter leading to a better or

worse coupling of the few photons. Therefore the shutter should always be placed on a damping surface to minimize the effect of the oscillations on the optical setup. Also all measured times should only be treated as a reference as the times vary for each setup, due to the exact positioning of the shutter.

To examine how reliable the shutter works, the variance of the recorded data was calculated and compared to the mean value. For this the variance was once plotted against the time (figure 4.9 (a) and (c)) and once it was plotted against the mean value ((b) and (d)) for both the rising and the falling slope of the pulse. Looking at the calculated variance (red points) in figure 4.9, we see that its always higher than the mean value (black points). Taking into account the already measured added noise of the laser source, we see that the modified variance (blue points) is nearly identical with the mean value, leading to the assumption that the shutter works highly reliable.

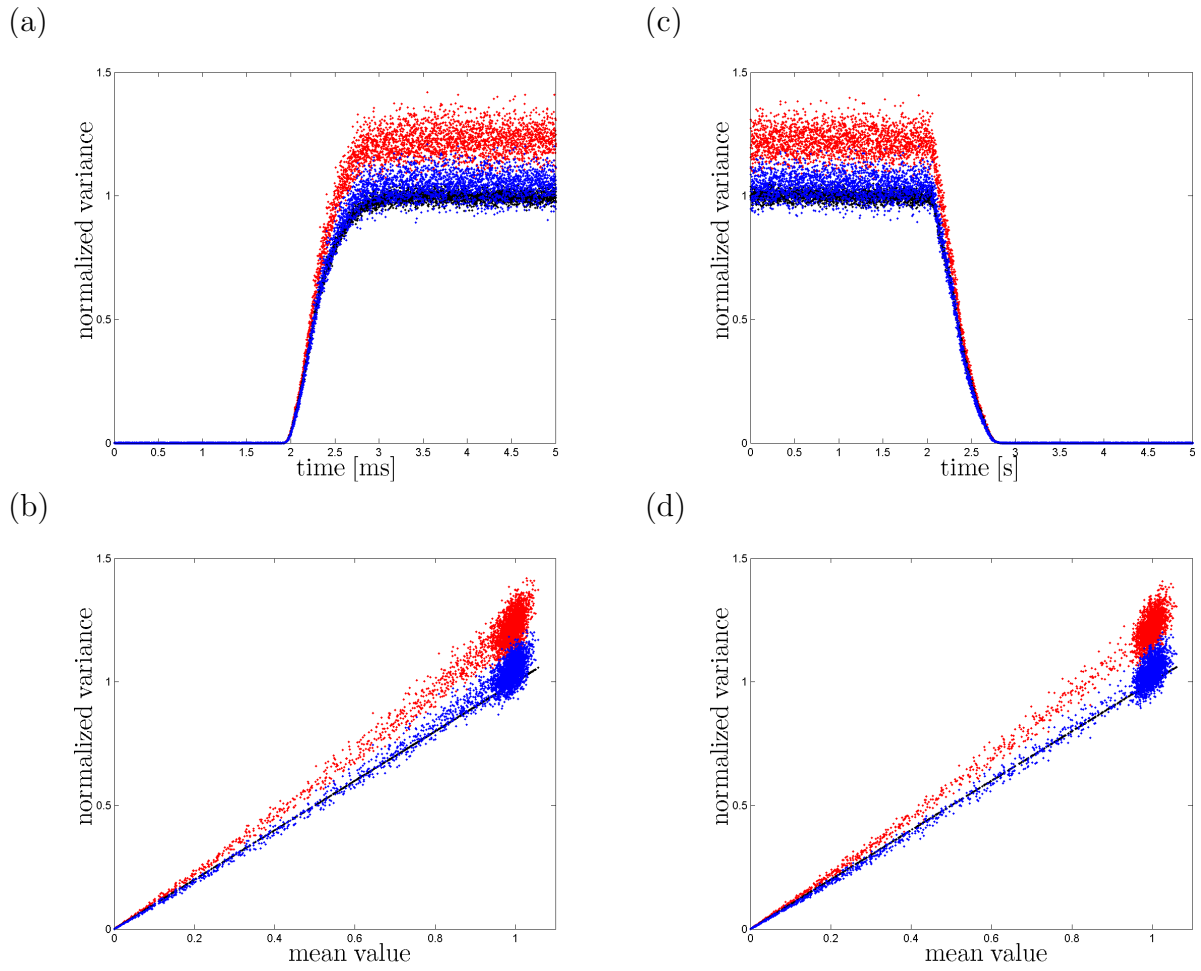

Figure 4.9: Calculated variance (red points) and modified variance (blue points) compared to the mean value (black points) for the opening shutter on the left and for the closing shutter on the right side.

In the last measurement performed with the mechanical shutter the laser beam was focused down to a beam waist of approximately 0.1 mm at the position of the shutter and then collimated again after the shutter. For this measurement there was again plotted the normalized counts with a fitting curve laid through the points, as it's shown in figure 4.10. For this the rise time was measured to be 71 µs and the fall time 49 µs. For the focused beam the impact of the exact positioning of the shutter is even greater than for the not focused beam. These times should as such only be treated as an order of magnitude measurement for shutter used in different setups.

(a) (b)

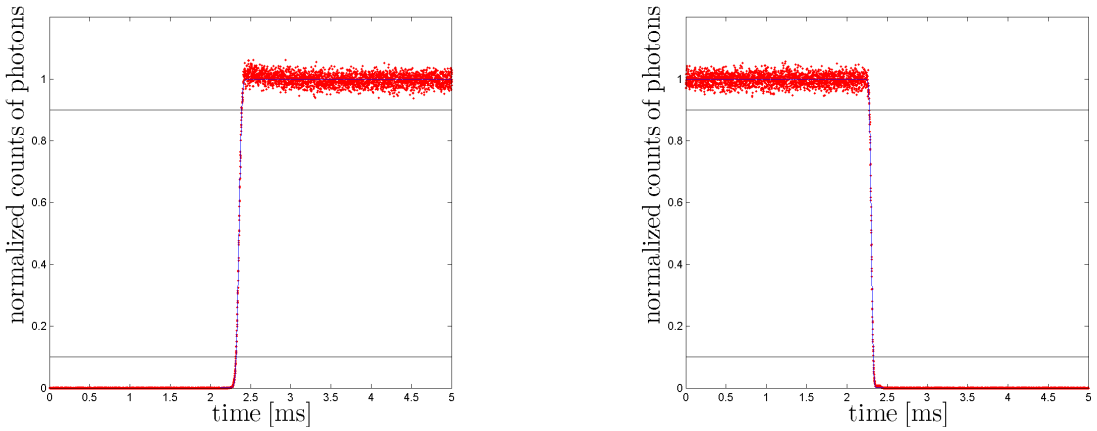

Figure 4.10: Rising and falling slope of a shutter pulse with a laser beam focused down to a beam waist of approx. 0.1 mm.

All in all the mechanical shutter was found to be very reliable, which is important for its application to avoid stray light. The rise and fall time of light pulses created by the shutter were found to be varying from around 50 µs up to 1 ms, heavily depending on the beam of light (focused or not) and the positioning of the shutter (angle between the initial position and the light beam).

4.4 AOM-Pulses

To create short pulses of light an AOM is used in most experimental setups. As described in the explanation of the AOM, the pulses are created by turning on and off the acoustic waves inside the medium of the AOM (a TeO_2 crystal), which interact with the light of the laser. As such the rise time of the light pulse depends only on the speed of the acoustic waves and the diameter of the light beam.

For the measurements the setup as shown in figure 4.11 was used. As light source the same laser as in the last part was used, again with the optical isolator at the beginning of the optical path. The change in the setup compared to the shutter measurements, are the lenses used to focus the light beam inside of the crystal of the AOM. This was done using lenses with different focal lengths (100 mm, 200 mm and 400 mm) as first lens f_1, while for the second lens f_2 a 100 mm lens was used. The setup was also used with no lenses and modified to a telescope type setup (reducing the beam radius to $1/2$ and $1/4$) in front of the AOM to achieve different values for the beam radius inside of the AOM.

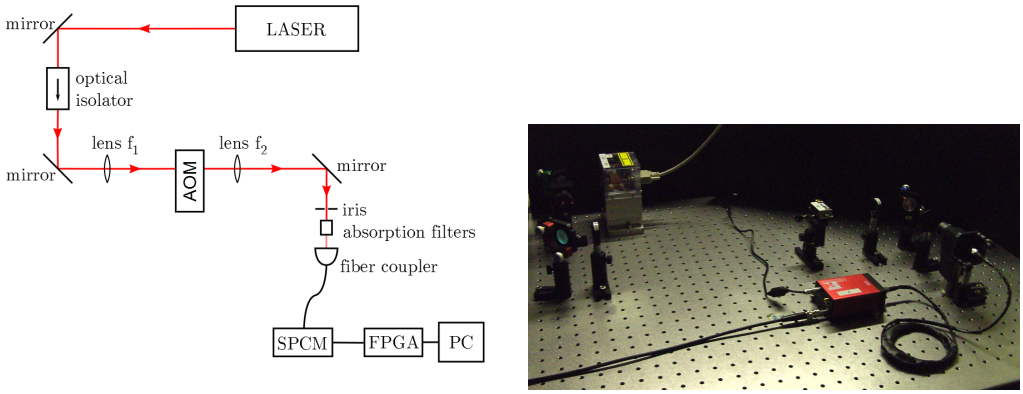

Figure 4.11: On the left side the schematic setup for the measruements, while on the right side a photo of the actual setup with an 400 mm lens as first lens is shown.

To compare the measurements performed with the AOM to the ones using the shutter a 1 s light pulse was created and recorded with the same resolution that was used for the shutter pulse. The comparison of the pulse created with an AOM (figure 4.12) with the one created by the shutter (figure 4.7) clearly shows that the rise and fall time of the AOM is significantly smaller. This is as expected due to the fact that the AOM uses acoustic waves to create the pulses of light instead of the mechanical means of the shutter.

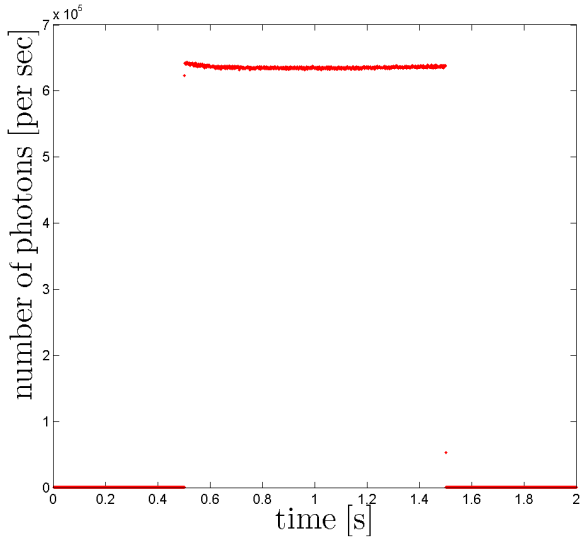

Figure 4.12: Measurement of a 1 s light pulse, measured to compare the AOM to the mechanical shutter.

As another important aspect the number of repetitions required to reconstruct a few-photon pulse with a high time resolution was examined. The impact of the number of repetitions on the pulse shape of a 50 ns pulse, recorded with a resolution of 100 ps is shown in figure 4.13 (a) and with a resolution of 1 ns in figure 4.13 (b).

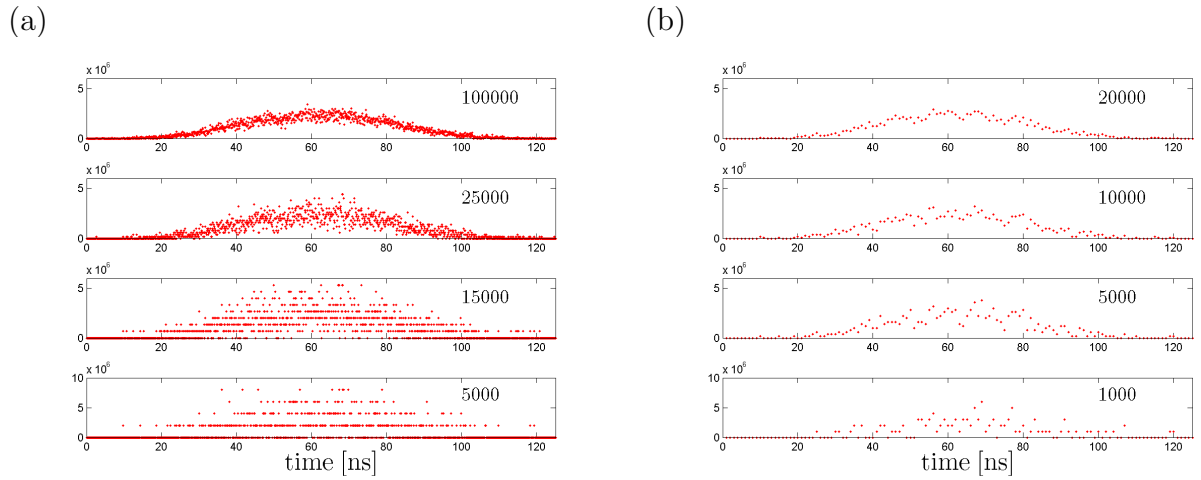

Figure 4.13: Impact of the number of repetitions used to recreate a 50 ns pulse measured with a time resolution of 100 ps (left) and with a resolution of 1 ns (right). For the time resolution of 1 ns the data of the 100 ps measurement was combined to the achieve the 1 ns bins during the analysis.

By decreasing the time resolution, and as such using longer bins, the necessary number

of repetitions to obtain a nice pulse shape also decreases, as shown in figure 4.13. For a counting rate of 1 Mio counts/s the mean value of a photon inside a 1 ns bins is only 0.001, which means only one of 1000 measurements should measure a photon for this bin. To obtain a reasonable mean value more than 1000 repetitions of the measurement are necessary. For a better time resolution (as shown in the figure for a bin width of 100 ps) even more measurements are necessary to achieve a reasonable mean value and as such a nice pulse shape.
Using the different lenses to achieve different beam waists inside of the AOM, the rise time (for the AOM the rise and fall time are the same and therefore the mean value of both will be stated) was determined using short pulses and a high resolution (down to 100 ps). Again an error function was used as a fit function for the normalized data, as its shown in figure 4.14 for a beam waist of 130 µm, achieved with a lens of 400 mm focal length as first lens.

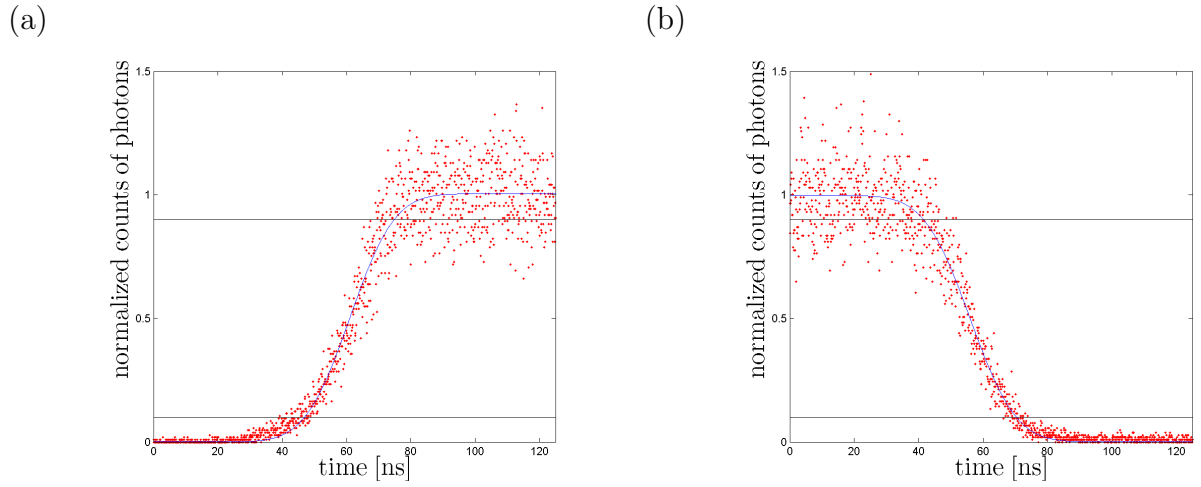

Figure 4.14: Measured data of the rising and falling slope of a light pulse created with an AOM and the respetive fitting function. The measurement was done with a lens of 400 mm focal length resulting in a beam waist of 130 µm.

All determined rise times that are shown in table 4.1 are mean values over two different measurements and over the rise and fall time of each measurement. In the table the times are also compared to the theoretical values, which can be calculated for a gaussian beam profile by taking the length the profile needs to include 80% of its intensity (which is $1.281552 \cdot w_0$) and dividing it by the speed of the sound waves.

$$t_{\text{rise}} = \frac{1.281552 \cdot w_0}{v_{\text{sound}}} \tag{4.3}$$

The speed of the acoustic waves inside the TeO_2 crystal of the AOM is specified as 4200 $\frac{\text{m}}{\text{s}}$ [11]. The size of the laser beam was measured with a CCD-Chip, leading to the values for the beam waists given in table 4.1.

beam waist w_0	measured t_{rise} [ns]	calculated t_{rise} [ns]
1.02 mm	368.5	311.2
510 µm	226.0	184.3
255 µm	122.8	92.1
130 µm	28.8	39.7
70 µm	15.6	21.4
150 µm	20.3	45.8

Table 4.1: Comparison of the measured rise times with their theoretical value for their respective measured beam waist

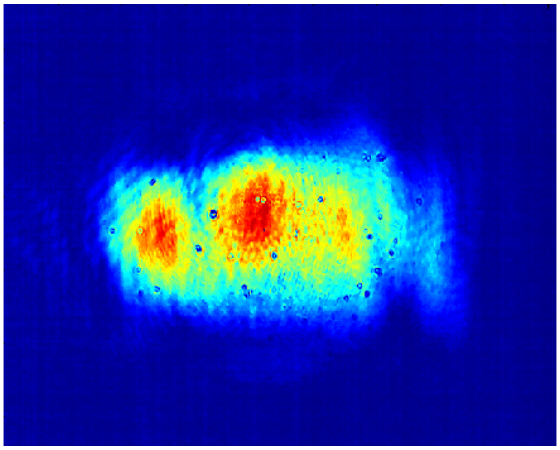

Figure 4.15: Intensity distribution of the laser beam, measured with a CCD-Chip.

As shown in figure 4.15 the used laser did not show a perfect gaussian profile and as such the obtained values for the beam waists from a gaussian fit differ from the actual beam waists. This explains the difference between the measured and the calculated rise times. Also seen in the table is that the waist for a bigger beam was measured to be to small, as the calculated rise times are smaller than the ones measured. This is as expected because the fitted gaussian to the intensity curve differed more for a broader beam than for the focused beams. Also the last value for the beam waist can't be correct, which most likely results from not hitting the focus of the 100 mm lens with the CCD-chip. All in all it can be said that the measured values roughly match with the theoretical rise times, showing that the measurement with the SPCM works properly.
The high time resolution of the measurement was then used to measure the delay between the electric signal and the light pulse and also to measure the speed of sound inside the crystal of the AOM. For this the laser beam was focused (therefore the 400 mm lens was used resulting in a beam waist of 130 µm) and then measurements of a 100 ns pulse were done, once when the light entered the AOM leftmost and once rightmost of the opening. The delay to the electric signal was measured by taking the side nearest to the piezoelectric transducer and determining the time distance to the electric signal, which is shown in figure 4.16 as black line at 0.4 µs. The delay was determined to be $\Delta t = 265$ ns and is caused by different factors summing up to the measured delay. The biggest factor is the signal propagation time of the electric signal through the used cables and the electric driver of the AOM, summing up to around 100 ns. Another factor is the delay between photon impact

and TTL-output of the SPCM, specified to be 50 ns. A relatively small part of a few ns is caused by the propagation time of the light from the AOM to the SPCM. The rest of the delay could be caused by the time the signal to the AOM needs to reach its full intensity (as the amplifiers in front of the piezoelectric transducer need a short time to reach their maximum output) or the time the sound waves need from the piezo to the opening in the AOM casing.

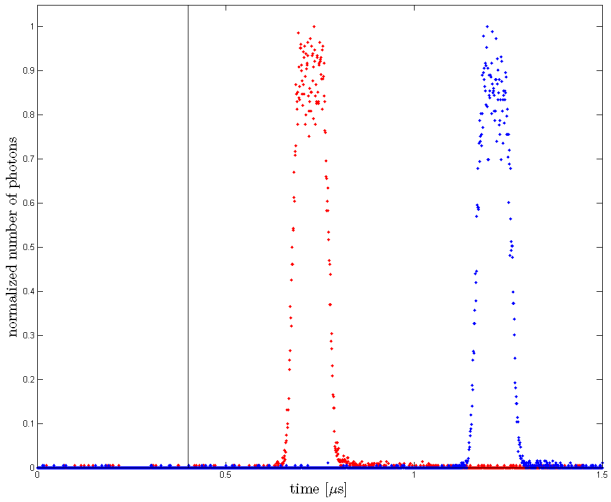

Figure 4.16: Measurements of a 100 ns pulse done to determine the delay between electric signal and light pulse and the speed of the sound in the quartz crystal.

As shown in figure 4.16 there is also a delay between the pulses, which were created by light passing through the AOM leftmost and rightmost of its opening. This delay is caused by the finite speed of the sound waves. The delay was taken from the figure to be $\Delta t = 488\,\text{ns}$. The opening of the AOM has the size of $2.5\,\text{mm} \times 1\,\text{mm}$, from which only the first value is relevant because that's the direction the sound waves take through the medium. The laser beam was focused down to a beam waist of 130 µm, which leads to a distance of about 2.24 mm between the two measurements. With these values the speed of the sound wave can now be calculated:

$$v_{\text{sound}} = \frac{\Delta s}{\Delta t} = \frac{2.24\,\text{mm}}{488\,\text{ns}} = 4590.2\,\frac{\text{m}}{\text{s}} \tag{4.4}$$

This obtained value differs by 9.3% from the specified value of $4200\,\frac{\text{m}}{\text{s}}$ [11], which is quite good considering the vague adjustment of the laser beam to the sides of the opening of the AOM by visual judgement.

4.5 Slow Light Measurements

As last part of this thesis the SPCM and the Time-Tagger were used to measure slow light. This was done for two different setups, once for the setup of the advanced laboratory EIT-experiment and once for the setup of the Rydberg Quantum Optics (RQO) group. In particular the delay of the RQO setup was determined.

4.5.1 Advanced Laboratory

The setup in the advanced laboratory already existed and only a few modifications were necessary for the desired measurements. As such the optical path had to be adjusted, so that the first order light from the AOM was used instead of the zero order. The second modification was the setup used to lock the probe laser (the coupling laser could already be locked). For this a spectroscopy of a Rubidium vapour cell was used to realize a dichroic-atomic-vapour laser lock (DAVLL)[6], with which the laser could be locked to the necessary transition.

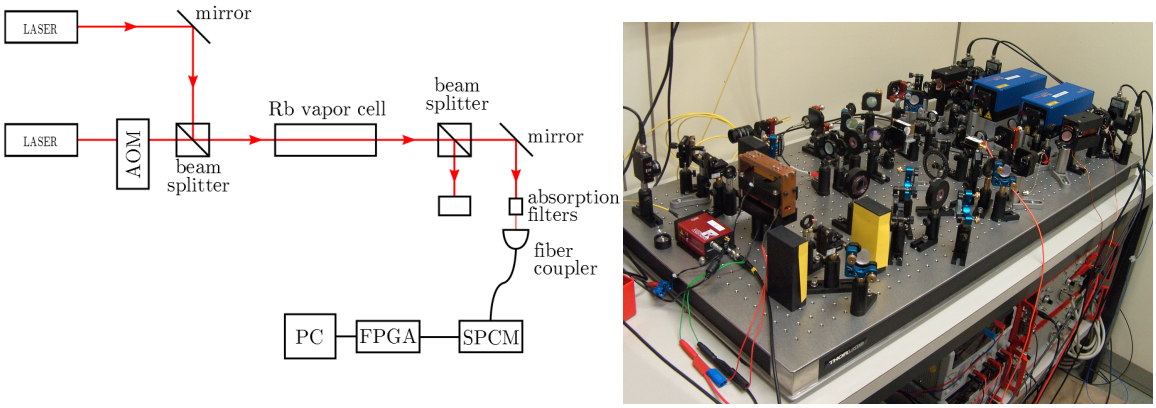

Figure 4.17: Simplified illustration and picture of the actual optical setup of the EIT measurements done in the advanced laboratory.

A simplified illustration and a picture of the actual setup is shown in figure 4.17. In this setup the Rubidium D_2-line was used to achieve the necessary 3-level system, as explained in the theory chapter. For this the ^{85}Rb-transitions were used, with the coupling laser frequency stabilized to the transition between the F = 3 hyperfine ground state and the hyperfine states of the $5\,P_{3/2}$ state. The frequency of the probe laser could be locked to and scanned through the transition between the F = 2 hyperfine ground state and the $5\,P_{3/2}$ state. The beam of the probe laser passed through an AOM, which was used to create the necessary light pulses. Both beams were superimposed with a beam splitter before passing

[6]For more information about the locking mechanism see [12].

through a Rubidium vapour cell, which was used as medium for EIT. After the vapour cell the two beams were splitted again, with the probe laser being attenuated and then coupled into a single mode fiber. The probe beam was also already attenuated before superposing it with the coupling beam, in order to fulfil the EIT condition $\Omega_p \ll \Omega_c$.
First of all the spectrum of the used transition was measured, once using a photodiode and once with the SPCM. The measured spectrum is shown in figure 4.18, with the red curve showing the absorption without the coupling field and the blue curve showing the EIT-spectrum.

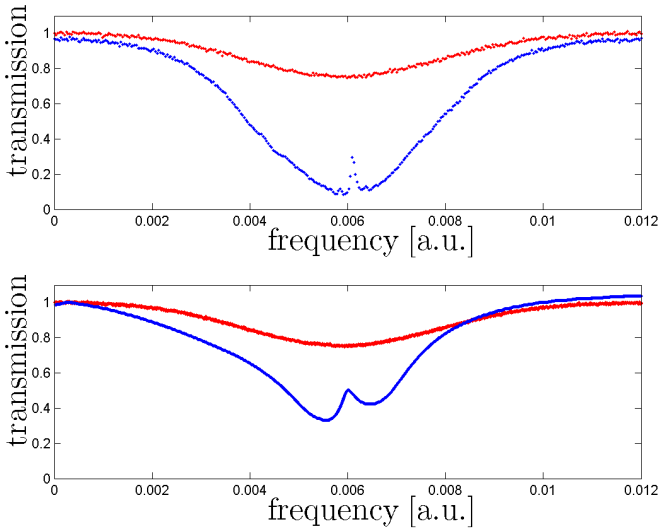

Figure 4.18: Observed transmission spectrum of the setup in the advanced laboratory without (red curve) and with the coupling field (blue curve).

The absorption with the coupling field turned on is considerably higher due to optical pumping effects caused by the coupling light. The depth of the absorption spectrum measured with the photodiode varys from the one measured with the SPCM, which was most likely caused by the fewer photons used for the SPCM measurement, as the probe beam was attenuated by a larger factor before passing through the vapour cell. It is also clearly visible that the measured height of the EIT peak is diminished by dephasing processes inside of the hot Rubidium gas.
The probe laser was then locked to the frequency of the EIT peak, with measurements done for slightly different positions of the frequency inside of the absorption valley. Some of these measurements are shown in figure 4.19. The black measurement looks to be the best position of the laser, while the blue and green ones show that parts of the pulse were absorbed leading to the change in the pulse shape. The red data points were measured with the probe laser highly detuned from any transition and as such showing no absorption. For these pulses the delay was determined by calculating the weighted mean value of the time for each pulse. For this the sum over the product of pulse height (photon counts) and

time was divided by the summed counts. Subtracting the calculated times for the slowed pulse (black) from the red pulse, a delay time of 7.02 ns was obtained. For the other two pulses higher delay times were calculated, caused mostly by the change in the pulse shape.

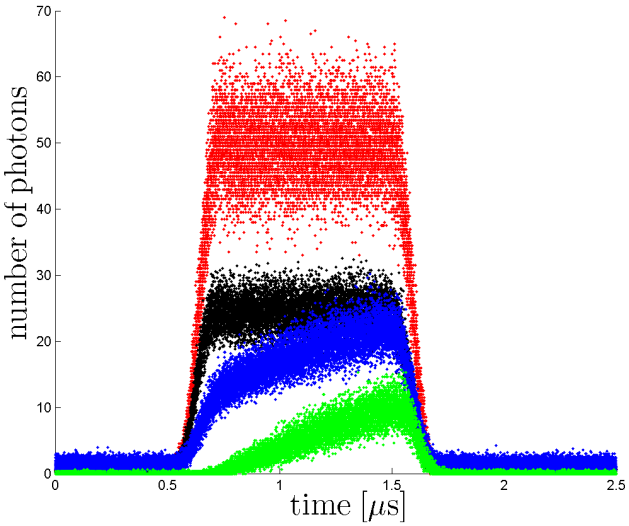

Figure 4.19: Measurements of the delay caused by the slow light. The red pulse shows the pulse without delay, whereas the other pulses show the delayed pulses each for a slightly different frequency.

With this delay time the achieved group velocity can be calculated with equation 4.5, which can be derived from equation 2.34.

$$v_g = \frac{1}{\frac{\tau_d}{L} + \frac{1}{c}} \tag{4.5}$$

With the length of the vapour cell ($L = 10\,\text{cm}$) the achied group velocity is 13598848 $\frac{m}{s}$. This corresponds to 4.54% of the vacuum speed of light.
As explained there were various problems during the measurements, such as the stability of the locking system for the probe laser or even the stability of the whole setup, as there were for example large drifts in the temperature during the day. Another point was the relative small EIT peak, leading only to small delay times, caused by dephasing effects in the hot vapour cell.

4.5.2 RQO experiment

In the RQO experiment EIT can be observed in a ladder-type system, with the upper state being a Rydberg state.

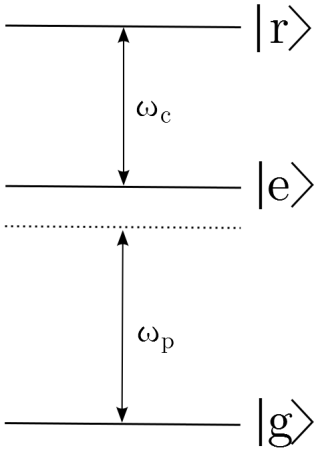

Figure 4.20: Level System of the RQO setup

The ground state shown in figure 4.20 is the $5\,S_{1/2}$ ground state of ^{87}Rb. As excited state $|e\rangle$ the $5\,P_{3/2}$ was used and for the Rydberg state the 40 S state. Therefore different lasers had to be used as coupling and probe laser. The blue laser, which acts as coupling field, is locked to be resonant to the transition from the $5\,P_{3/2}$ to the 40 S Rydberg-state. This transition corresponds to a frequency of 623.3724 THz. The frequency of the red laser used as probe laser can be changed by locking it to a set value and changing the value for each cycle of the experiment. As described in the theory section this system only shows EIT on the few photon level for the high optical density achieved in the atomic cloud and as such all the absorption filters were placed at the beginning of the optical path of the probe laser.
This setup uses a cold cloud of ^{87}Rb atoms as medium for EIT. The cloud of atoms is created by loading Rubidium atoms from a gas, which was created through evaporation, into a magneto-optic trap (MOT). After loading the atoms from the MOT in a dipole trap, the generated cloud is roughly 100 µm in diameter and its temperature in the range of 40 µK. Turning off the dipole trap the cloud expands freely and in this time the actual experiment is done. After letting the cloud expand for 1 ms the whole procedure is repeated, leading to a cycle of about 4 s.
The EIT spectrum of the expanding ^{87}Rb cloud is shown in figure 4.21. To obtain this spectrum the frequency of the probe laser was changed by 0.2 MHz after each cycle of the experiment. For each step of the frequency the photon count is measured for multiple bins, each with a length of 20 µs. As the cloud expands its density decreases and as such the later bins show the spectrum of a lower density. As such the spectrum is registered for different densities. In the case of the spectrum in figure 4.21, the first 5 bins were combined, leading to a mean value of the spectrum for the first 100 µs of the expansion of the cloud with a fit function laid through the measured points.

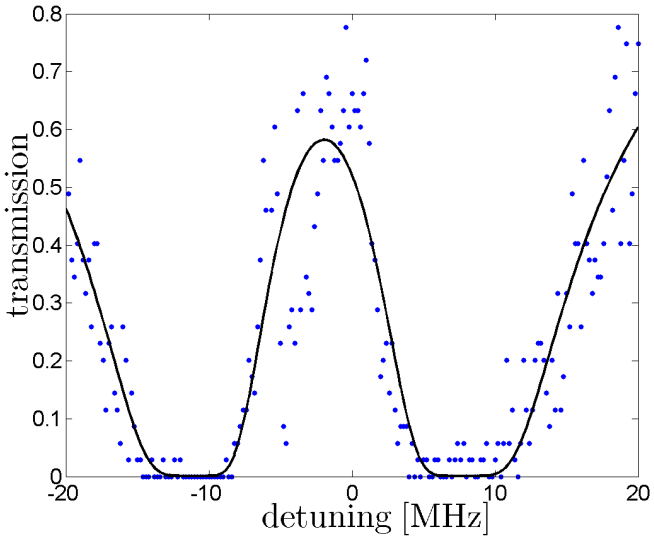

Figure 4.21: Obtained EIT spectrum of the RQO experiment measured in a region of 40 MHz around the two-photon resonance.

For the measurements of slow light the probe laser was locked to the frequency of the maximum of the EIT peak. For this fixed frequency pulses of 1 µs length and a distance of 2 µs between each other, were created using a pulse generator and an AOM. During one cycle of the experiment 100 such pulses were sent through the expanding cloud and also when no atoms were present. During the analysis of the data 10 of the pulses were combined and then plotted, leading to figure 4.22 in which four of the 10 resulting pulses are shown as an example.

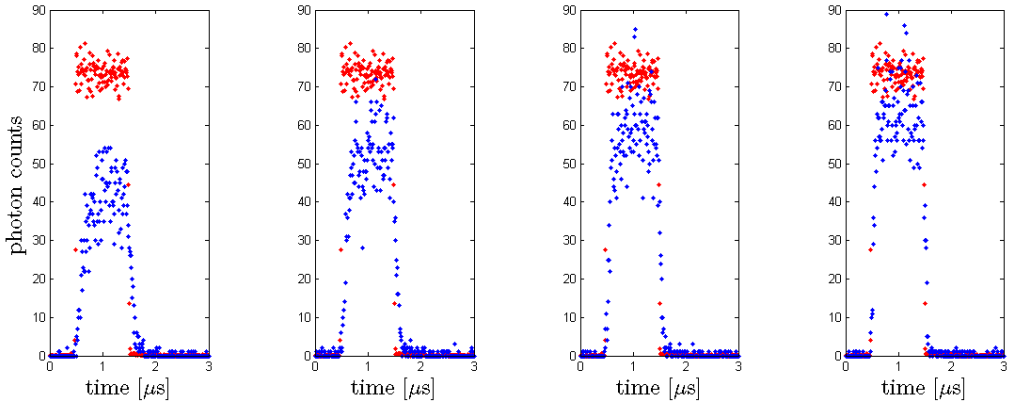

Figure 4.22: Illustration of the delay caused by the slow light effect. The red pulses shows the pulse without delay, whereas the blue pulses show the delayed pulses obtained by combining the pulses 1-10, 21-30, 41-50 and 61-70.

From the figure it is clear to see that the transmission through the cloud increases with the decreasing density, as the later pulses are higher then the first ones. For all recorded pulses the delay time was calculated as explained in the previous section. These delay times were then plotted against the number of the pulse (and as such against the density of the cloud), showing a decrease in the delay the smaller the density of the cloud. Also for each pulse the obtained group velocity was calculated with equation 4.5 with a cloud length of 100 µm. These obtained group velocities were again plotted against the number of the pulse, as shown on the right side of figure 4.23.

(a) (b)

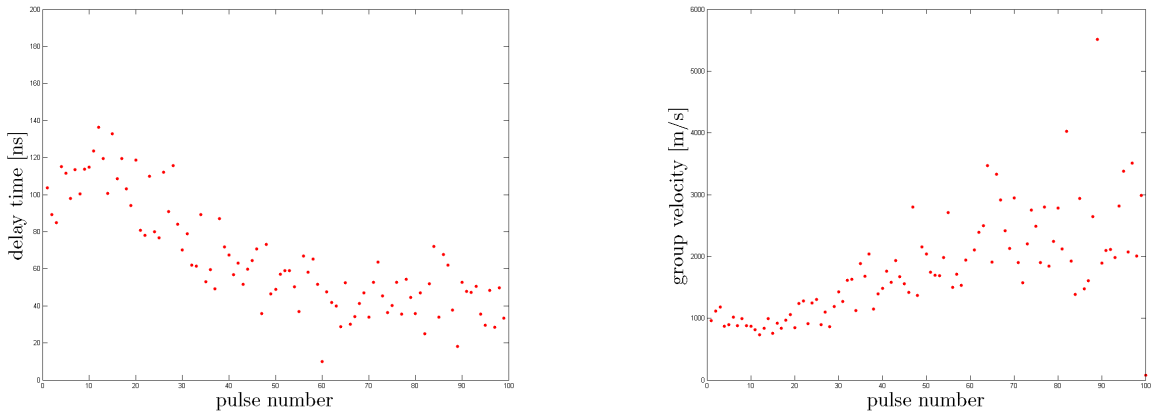

Figure 4.23: Obtained delay times (a) and calculated group velocities (b) for each pulse.

These two figures show that the delay between the pulses decreases with the decreasing density, corresponding to a smaller slope in the EIT spectrum. This decrease in the delay time leads to the observed increase of the group velocity. Calculating the mean value of the group velocity for the first 20 pulses, we obtain a value of 921.6 $\frac{m}{s}$. This corresponds to $1/325300$ of the vacuum speed of light. This is clearly a better result as the one obtained in the hot vapour cell, which is due to fewer dephasing effects inside the clod cloud than in the hot vapour.
All in all the measurements of this section show that the effect of slow light leads to measurable delay times, caused by the reduction of the group velocity of a light pulse inside a medium showing EIT.

5 Summary and Outlook

The aim of this thesis was to work with and test the single photon counting modules and the high resolution timing with the Time-Tagger. The measurements done during this thesis show that both of these modules work properly and that they can be used together to reconstruct light pulses from the measurements of few photons. It was also show that it is possible to measure the delay caused by slow light with these pulse measurements, as it was done in particular for the RQO experiment.
To obtain this conclusion it was first shown that the measured dark count rates of both SPCM's agreed with their specified values. Next the photon statistics of laser light was investigated leading to the detection of added noise in the measurement. Whether this noise comes from the laser source or the measurement/analysis itself couldn't be finally proved during this thesis and should be examined again.
As next step a mechanical shutter was used to create pulses of light with rise and fall times varying from around 50 µs up to 1 ms depending on the beam of light and the positioning of the shutter. By considering the variance of the recorded data and by taking the already measured added noise into account, the shutter was found to be highly reliable.
Afterwards light pulses were created using an AOM, leading to considerably shorter rise times of around 20 ns up to 370 ns. These measured values agree in their order of magnitude with the once calculated. The measurement of light pulses was then used to determine the speed of sound inside the crystal of the AOM, with the determined value agreeing in its order of magnitude with the specified value.
As last part of this thesis a SPCM was used to measure the delay of light pulses inside an EIT medium. This was done for a hot Rubidium vapour cell and for a cold cloud of Rubidium atoms, clearly showing better results in the cold cloud due to fewer dephasing effects. For the light pulses delay times in the order of 100 ns were measured, corresponding to group velocities of 1000 $\frac{\mathrm{m}}{\mathrm{s}}$ inside the atomic cloud.

During the process of this thesis the SPCM's were already used to measure EIT spectrums of the cold Rubidium cloud of the RQO group. In the future it will be tried to use the strong long-range interactions of the Rydberg states and the strong atom-light interaction of EIT to control the quantum state of the light. As mentioned above in the text the excitation of one Rydberg state leads to a shift in the energy levels of the surrounding atoms inside the blockade volume. For a second photon passing through the medium, the system is then effectively a 2-level system, leading to the absorption of the photon. This can be used to create a single-photon switch or even a single photon source and as such the SPCM's will be needed to verify the non-classical nature of the output light.

Acknowledgements

I would like to thank everybody who helped me during the creation of this thesis. In particular I want to thank:

- Prof. Dr. Tilman Pfau, for the opportunity of doing this thesis in the 5th institute.
- Dr. Sebastian Hofferberth, for being the supervisor of this thesis and always being there to answer questions and to help when needed.
- Christoph Tresp and Hannes Gorniaczyk, who were always there whenever I needed help or advice.
- Michael Schlagmüller, Huan Nguyen, Thomas Schmid and Dr. Graham Lochead, who all worked at the experiments in the 5th floor during this thesis and were also always there for questions.

Bibliography

[1] Mark Fox, *Quantum Optics, An Introduction*, Oxford University Press (2006)

[2] Rodney Loudon, *The Quantum Theory of Light*, Oxford University Press (2000)

[3] Micheal Fleischhauer, Atac Imamoglu and Jonathan P. Marangos, *Electromagnetically induced transparency: Optics in coherent media*, Reviews of Modern Physics Volume 77 (April 2005)

[4] Stephen E. Harris, *Electromagnetically Induced Transparency*, Physics Today (July 1997)

[5] L.V. Hau, S.E. Harris, Z. Dutton and C.H. Behroozi, *Light speed reduction to 17 metres per second in an ultracold atomic gas*, Nature Vol. 397 (18. February 1999)

[6] T. Peyronel, O. Firstenberg, Q. Liang, S. Hofferberth, A.V. Gorshkov, T. Pohl, M.D. Lukin and V. Vuketić, *Quantum nonlinear optics with single photons enabled by strongly interacting atoms*, Nature Vol. 488 (2. August 2012)

[7] Daniel Adam Steck, *Rubidium 85 D Line Data*, `http://steck.us/alkalidata/rubidium85numbers.pdf`, Version 2.1.5 (3. August 2013)

[8] Daniel Adam Steck, *Rubidium 87 D Line Data*, `http://steck.us/alkalidata/rubidium87numbers.pdf`, Version 2.1.4 (3. August 2013)

[9] Laser Components, *Data sheet and specifications of the COUNT-250C-FC modules*

[10] Udo Hermann, *A nanosecond-resolution computer control system for deterministic excitation of Rydberg superatoms*, Bachelor thesis (2012)

[11] Crystal Technology Inc., *Datasheet of the AOM*, `http://www.goochandhousego.com/products//modulatorsdatasheets/3080-122%2897-01280-01rD%29.pdf` (3. August 2013)

[12] Kristan L. Corwin et al. , *Frequency-stabilized diode laser with the Zeeman shift in an atomic vapour*, Applied Optics Vol. 37, No. 15 (May 1998)

[13] T. Zou and L. Mandel, *Photon-antibunching and sub-Poissonian photon statistics*, Physical Review A Vol. 41, 475 (January 1990)